

Close-Range Photogrammetric Measurement of Static Deflections for an Aeroelastic Supercritical Wing

Thomas A. Byrdsong, Richard R. Adams,
and Maynard C. Sandford
Langley Research Center
Hampton, Virginia



National Aeronautics and
Space Administration
Office of Management
Scientific and Technical
Information Division

1990

1. The first part of the document discusses the importance of maintaining accurate records of all transactions and activities. It emphasizes that this is crucial for ensuring transparency and accountability in the organization's operations.

2. The second part outlines the specific procedures for recording transactions, including the use of standardized forms and the requirement for double-checking entries to prevent errors.

3. The third part addresses the role of the accounting department in managing these records, highlighting the need for regular audits and the implementation of robust internal controls.

4. The fourth part discusses the challenges associated with maintaining accurate records, such as the risk of data loss or corruption, and provides strategies to mitigate these risks.

5. The fifth part concludes by reiterating the importance of accurate record-keeping and encourages all staff members to adhere to the established procedures.

Summary

Close-range photogrammetric measurements were made for the lower surface of an aeroelastic supercritical research wing having a full-span aspect ratio of 10.3. The measurements were made during wind-tunnel tests of quasi-steady pressure distributions on the wing. The tests were conducted in the Langley Transonic Dynamics Tunnel at Mach numbers up to 0.900 and dynamic pressures up to about 300 psf. Deflection data were obtained at 57 locations on the wing lower surface with dual nonmetric still-frame cameras. Representative data are presented as a graphical overview to show variations and trends of spar deflection with test variables. Comparative data are presented for photogrammetric and cathetometric results of measurements of the wingtip deflections.

Introduction

The Langley Research Center has conducted an aeroelastic research wing program to evaluate transonic aerodynamic computer codes for the prediction of lifting surface loadings. The research program consisted primarily of wind-tunnel measurements of steady and unsteady pressure distributions on wing models and correlation of these measurements with computational results. Quasi-rigid and flexible semispan wing models were used in the wind-tunnel tests. Thus far, three quasi-rigid models have been tested in the Langley Transonic Dynamics Tunnel: a delta wing model (ref. 1), a swept wing model with supercritical airfoil sections (ref. 2), and a rectangular wing model with a supercritical airfoil (ref. 3). These models were designed and fabricated to minimize structural dynamic effects and, accordingly, to simplify correlation of the experimental data with computational results.

More recently, wind-tunnel measurements have been completed for a fourth model of the aeroelastic research wing program (refs. 4 through 6). Both static and dynamic data were obtained for this highly flexible wing which was designed for a flight-test program to evaluate active control systems. Selected results from dynamic pressure measurements for the flexible wing are reported in references 5 and 6, and the measured static pressure data are currently being analyzed. The measured static pressure distributions were supplemented with corresponding measurements of wing surface deflections to provide for more meaningful results.

The purpose of this paper is to document the results of wing surface deflection measurements for their corresponding wing surface static pressure measurements. The documentation presented herein

graphically shows variations of the primary wing spar shapes and wingtip deflections as a function of the various test variables to provide views of the trends developed in the data. Tabulations of all wing surface deflection measurements are presented in a "Supplement to NASA Technical Memorandum 4194," which is available on request, for use in evaluation of theoretical techniques under development. A request form is included at the back of this report. Wing surface deflection measurements were obtained for a range of Mach number from 0.600 to 0.900, a range of angle of attack from -2° to 4° , a range of control surface deflection from -8° to 8° , and dynamic pressures up to about 300 psf. Wing deflections at 57 locations were obtained with two nonmetric still-frame cameras synchronized to an electronic flash. Cathetometric measurements of some of the wingtip deflections were also obtained. The tests were conducted in a heavy gas medium.

Symbols

| | |
|-------------|--|
| a_0 | Y-axis intercept of linear equation |
| a_1 | slope of linear equation |
| b | wing semispan, in. |
| C_{cor} | correlation coefficient |
| c | wing streamwise local chord, in. |
| M | free-stream Mach number |
| p_s | static pressure, psf |
| p_t | stagnation pressure, psf |
| q | free-stream dynamic pressure, psf |
| T | stagnation temperature, $^\circ R$ |
| X_S | streamwise spatial coordinate, in. |
| $X_{S,rms}$ | estimated root-mean square precision of spatial coordinate X_S |
| x_c | streamwise station coordinate for each camera, in. |
| x_l | local streamwise distance from wing leading edge, in. |
| Y_S | spanwise spatial coordinate, in. |
| $Y_{S,rms}$ | estimated root-mean-square precision of spatial coordinate Y_S |
| y_c | lateral station coordinate for each camera, in. |
| y_l | perpendicular distance from wing line of symmetry, in. |
| Z_S | vertical spatial coordinate, positive up, in. |

| | |
|--------------|--|
| $Z_{S,avg}$ | average value of targets $Z_{S,1002}$ and $Z_{S,1004}$ relative to wind-off value of corresponding Z_S , in. |
| $Z_{S,C}$ | cathetometric measurement of vertical spatial coordinate Z_S relative to wind-off condition, in. |
| $Z_{S,P}$ | photogrammetric measurement of vertical spatial coordinate Z_S relative to wind-off condition, in. |
| $Z_{S,rms}$ | estimated root-mean-square precision of spatial coordinate Z_S |
| $Z_{S,1002}$ | vertical spatial coordinate of target 1002, in. |
| $Z_{S,1004}$ | vertical spatial coordinate of target 1004, in. |
| z_c | vertical station coordinate for each camera, in. |
| α | angle of attack of model at wing root chord, positive leading edge up, deg |
| δ | static angle of outboard control about hinge line, positive leading edge up, deg |
| η | wing nondimensional semispan station, y_l/b |
| θ | elevation angle of orientation for each camera, deg |
| ϕ | roll angle of orientation, deg |
| ψ | azimuth angle of orientation for each camera, deg |

Abbreviations:

| | |
|--------|------------------|
| rms | root mean square |
| W.O.Z. | wind-off zero |

Model

Views of the test configuration mounted in the Langley Transonic Dynamics Tunnel are shown in figures 1 and 2, and the wing planform and photogrammetric targets mounted on the wing lower surface are shown in figures 3 through 5. The wing had a full-span aspect ratio of 10.3 and a leading-edge sweep angle of 28.8°. The wing was equipped with three trailing-edge control surfaces (figs. 3 through 5) that were hydraulically driven. Two of the control surfaces were located near the root chord and one was located near the tip chord. Location coordinates for

the control surfaces are shown in figure 4. The inboard control surfaces were fixed at a deflection angle of 0°, and the outboard control surface was deflected to predetermined static angles in the approximate range from -8° to 8°. Only the deflection angle of the outboard control surface was varied during this study. The hinge line of the outboard control was located at 77 percent of the local wing chord. The wing front and rear spar centerlines were located on the 25-percent and 62-percent chord lines on the basic wing planform, respectively (fig. 5).

The wing contour was formed by three supercritical airfoil sections that were located at wing nondimensional semispan stations η of 0.071, 0.426, and 1.000, and the corresponding airfoil thickness-to-chord ratios were 15 percent, 12 percent, and 11 percent, respectively. Straight line interpolation along constant-percent chord lines defined the wing contour between the three airfoils. The airfoil coordinates and twist distribution for the wing cruise condition are defined in reference 7, and additional geometric and structural characteristics are given in reference 4.

Circular targets were located on the wing lower surface (fig. 1) to define the surface deflection (or shape). The inboard rows of targets were orientated perpendicular to the rear spar in order to facilitate comparisons with structural analysis programs. The rows near the model tip were orientated streamwise to facilitate comparisons with aerodynamic analysis programs. Sixty-five targets were provided; however, only 57 targets were visible for the deflection measurements. The visible target locations on the wing lower surface are identified in figure 3. The targets, which are commonly used for printed circuit artwork, were dark red in the shape of an annulus with an outside diameter of 1 inch and a thickness of 5 mils. The white painted wing surface visible at the center of the pads provided the required high contrast target for the photographic images. Specular reflections were minimized by use of an over-spray of clear flat lacquer. The central hole diameters in the pads were selected to present constant image sizes of about 100 micrometers on the films as photographed by the inboard cameras. The central hole diameter ranged from 65 mils for the inboard targets to 125 mils for the outboard targets. The visible targets were located on the wing in 10 semispan rows between the wing root and tip and at up to 8 chordwise positions. The wing target locations from surface table measurements are shown in table 1. The corresponding target coordinates corrected for the axis system used in the photogrammetric data reduction are shown in table 2. A description of the corrections in table 2 is discussed in the section "Data Reduction." An

additional set of 18 high-contrast targets was placed on the test-section wall opposite the model mount within the field of view of each camera. These data were used to provide a basis for image restitution in the absence of film fiducial marks.

Boundary-layer transition strips were placed on the wing upper and lower surfaces for selected test conditions. The transition strips were 0.10 inch wide and were made of No. 70 Carborundum grit embedded in a plastic adhesive. The size and location of each strip were determined from experiences gained by using transition strips on similar wind-tunnel models. The strips were located on the 5-percent chord line from root to tip of the basic wing planform. The model surface forward of the strips was kept smooth to maintain laminar flow.

Instrumentation

Wing deflection data were recorded simultaneously on photographic film by use of two still-frame 70-millimeter square-format nonmetric cameras that were rigidly mounted behind high-strength glass windows in the test-section sidewall approximately 26 inches below $Z_{S,avg}$ of the wing coordinates. (See fig. 1.) The cameras were separated by a distance of 41 inches and were fitted with 50-millimeter focal-length lenses focused to a distance of 5 feet. Illumination was provided by a high-intensity strobe lamp located behind a window beneath the wing. Exposures were made remotely upon command by a control room observer. A logic circuit was used to assure that both camera shutters were open before allowing the strobe lamp to trigger. Seventy frame pairs could be exposed before film magazine reloading was required.

The relative vertical deflection of the wingtip was measured by use of a cathetometer to provide quick-look information. The cathetometer was mounted in the wind-tunnel control room behind windows of high-strength safety glass which provided a direct view of the test configuration (fig. 2). A horizontal line was drawn on the wingtip that approximated the wingtip chord line. During the test an orthogonal hairline system in the cathetometer optics was focused on the wingtip chord line for relative vertical displacement measurements.

Wind Tunnel

The test was conducted in the Langley Transonic Dynamics Tunnel (ref. 8). This facility is a single-return wind tunnel that has a 16.00-foot square test section with cropped corners. The test section walls, ceiling, and floor are equipped with streamwise longitudinal slots. The stagnation pressure can be

varied from slightly above atmospheric pressure to near vacuum over the Mach number range from 0 to 1.2. The tunnel is a continuous-operation type and is powered by a motor-driven fan. Both test section Mach number and dynamic pressure are continuously controllable. The facility has the capability to use air or heavy gas (R-12) as a test medium. Heavy gas was used as the test medium for most of these test runs.

Data Reduction

Data reduction of the wing surface deflection measurements was accomplished by use of the theory of photogrammetry. The theory is based upon a pair of equations (referred to as the projective equations) which relate the two-dimensional measured coordinates (x, y) of a film image and the corresponding three-dimensional spatial coordinates (X_S, Y_S, Z_S) of the target photographed. For this test program, the projective equations for each camera contained a total of 14 projective parameters (or elements of orientation). The calibration required for these measurements consisted of recovery of eight internal elements of orientation (referred to as the camera parameters) for each camera and six external elements of orientation (or station parameters) for each station. The camera parameters consisted of the principal distance of the lens, the image coordinates of the principal point, and five additional parameters which include three radial and two decentering lens distortion coefficients for each camera. The station parameters consisted of three station coordinates and three pointing (or orientation) angles for each camera station. A nonstandard technique was developed for image restitution due to the use of nonmetric cameras to record wing deflections. Also, the use of such cameras prevented removal of image errors that were introduced by film dimensional changes. A detailed discussion of the theory, equations, and the self-calibration process used in close-range photogrammetry is presented in reference 9.

Photographic Methods

Two sequences of photographs of the model (photographic calibrations) were made prior to testing. The first sequence was referred to as the self-calibration photography, and the second sequence was referred to as the angle-of-attack calibration photography. The required photographs for each sequence were obtained sequentially and only after completion of both sequences were the films removed from the cameras and processed.

Self-calibration photography. The self-calibration photography sequence of photographs was used to provide the data to recover the internal elements of orientation for the two cameras and

to provide coordinates of the wing targets in a properly scaled (but arbitrary) wing coordinate system. The targeted wing ($\alpha = 0^\circ$) was photographed in the test section with each camera from six locations that were circumferentially distributed beneath the wing. The cameras were rolled about their lens axes a different amount for each photograph. Finally, the self-calibration sequence was completed by mounting and locking the two cameras into their permanent test positions behind the tunnel windows beneath the wing and taking a seventh and final photograph of the targeted wing lower surface (fig. 1(b)).

Angle-of-attack calibration photography.

The angle-of-attack calibration photography sequence of photographs was used to provide the data to transform the resulting wing coordinate system (obtained from the self-calibration photography) into a preferred wing coordinate system and to remove the rigid-body rotation component from the data. Also, image coordinate data were obtained from this sequence of photographs for the 18 additional targets that were located on the tunnel side wall. Seven pairs of photographs were taken of the test wing and wall target grid from each camera as angle of attack was varied in increments of approximately 1° in the interval from -2° to 4° .

Film Measurement

Two-dimensional coordinates from the film were obtained for each target image on each film negative subsequent to film processing. Multiple readings of each coordinate were manually obtained by a precision monocomparator that was monitored by a microcomputer. The computer was programmed to accept the data when two successive measurements of each target (both x - and y -coordinates) were repeated within 10 micrometers. Coordinates of visible frame corners were also measured. Long-term instrument drift was found to exist in the comparator system; this drift was also monitored for each negative. The data were discarded when the coordinates of the first target measured differed by more than 15 micrometers when reread after reading all other targets. Seventy-five targets were measured on each film negative. Calibration and test photography generated a total of 700 negatives which required considerable manual comparator observation.

Image Data Preprocessing

The use of nonmetric cameras which lack discrete fiducial marks precluded the use of a direct standard two-dimensional coordinate transformation to convert raw image coordinates from an arbitrary com-

parator axis system to the conventional X - Y fiducial axis system. To overcome this difficulty, the frame corner data were used for this transformation. The four square-frame corners of each negative were measured for self-calibration and angle-of-attack sequences. In these cases, the origin was established at the computed intersection of the frame diagonals. The orientation was then fixed by an in-plane rotation about the new origin to place the reference frame edge parallel to the abscissa axis.

For test photography, it was necessary to operate under reduced test section ambient lighting to insure that fast strobe illumination predominated the exposures for the moving targets. Only two corners of the reference edge of each frame were measurable. These corners were used to establish the reference edge. In this case, the origin was temporarily established at the right angle apex opposite the reference edge (hypotenuse) of a 45° triangle. The image quality of the frame corners was insufficient to allow scaling of image data. The image data were then corrected for systematic comparator errors.

The final step in preprocessing of the image data involved the wall target image data that were obtained from the angle-of-attack photograph sequence. The quality of the wall target image data was quite good and resulted in highly repeatable image coordinates. The good quality of the wall target images was attributed to photographic exposure under high ambient illumination levels. Since the wall target grid appeared in all subsequent test photographs, their image coordinates were utilized (in lieu of fiducial marks) for the final image plane transformation of test image data. Subsequently, all image data from each camera frame (not including self-calibration photographs) were transformed to best overlay, in a least-squares sense, the images from this target subset. Again, the transformation was confined to the image plane (two translations and one rotation) and the scale was held fixed.

Wing Deflection Data Processing

Simultaneous Triangulation and Resection System (STARS, ref. 10) photogrammetric software was used to analyze the preprocessed image data. Individual modules of this software were utilized as follows to produce the desired results.

Self-calibration. Preprocessed image data from the self-calibration photographic sequence were merged, and a two-camera bundle adjustment (refs. 9 and 10) with self-calibration was performed. This procedure involved the solution of 1960 projective equations for 310 unknowns. Absolute control for this adjustment was established by use of known

X, Y, Z coordinates of two inboard wing targets (102 and 105) and the Z -coordinate of an outboard wingtip target (1003) as given in table 1. These three control points (targets 102, 105, and 1003) define a unique spatial coordinate system. The STARS bundle adjustment not only recovered the internal elements of orientation (principal distance, principal point location) for each camera, but also the lens distortion coefficients and external elements of orientation (the three station coordinates and the three pointing angles) for each camera station. The X, Y, Z coordinates for all targets in the system defined by the control points were also recovered from the adjustment. However, rather than generate a reference coordinate system from three selected control points, a preferred wing coordinate system was generated with all the measured data of table 1. This was accomplished in a least-squares formulation with the STARS Rigid Body Transformation module (ref. 10).

Since the scale was allowed to adjust during the transformation and a knowledge of the external elements of orientation of the two fixed camera stations was required for subsequent steps, the bundle adjustment was repeated with the control point coordinates fixed to the values obtained from the rigid body transformation. Rigorous error propagation emerged directly from the least-squares bundle adjustment (ref. 9). The Z -coordinates for the wing targets in the preferred wing coordinate system were recovered from this 14-station least-squares adjustment to an estimated rms precision of 0.0045 inch.

Angle-of-attack calibration. The wing was tested at various angles of attack with the camera stations fixed in the preferred coordinate system. The resulting X, Y, Z coordinates of the wing targets contained both the desired wing deformation data and the angle-of-attack rotation component. The angle-of-attack calibration was thus used to provide a means for separating the rotational component from the deformation data.

The preprocessed image data obtained from the angle-of-attack photographic sequence were merged in pairs and the STARS Triangulation module was used to obtain X, Y, Z coordinate sets at each of seven calibration angles of attack. The projective parameters used for the triangulation were those determined from the self-calibration. Since the wing was assumed to be a rigid body for this calibration sequence, the only variable between the resulting data sets was the angle-of-attack rotation. To verify that this was the case, a rigid body transformation (with scale fixed) was performed to best overlay the triangulated data sets from the two extreme angles of attack (-2° and 4°). The result of this transforma-

tion showed that the differences between the transformed set and the primary set were minimal. Also, this result verified that the actual coordinate system and the preferred wing coordinate system (as previously obtained) were not precisely mutually orthogonal. The coordinate system was corrected so that the Y -axis in the wing coordinate system was parallel to the axis of rotation in the tunnel system for changes in angle of attack. Once mutual orthogonality between the two systems was established, three final translations were made to adjust the preferred wing system to the actual tunnel system. The final coordinates of the wing targets in the tunnel coordinate system at zero angle of attack and the wind-off condition are given in table 2. The Z -precision estimates (table 3) reflect the overall effect of uncorrected image measurement errors—propagated through the recovery of the projective parameters—to the triangulated results from the pretest calibrations.

The corrected target coordinates (table 2) were collectively used as a control for a final bundle adjustment, using the preprocessed image data for the seven calibration angles of attack. All targets participated equally (in a least-squares sense) in the adjustment; effectively the previously established tunnel coordinate system was preserved. Except for the camera principal points, the internal elements of orientation and lens distortion parameters were rigidly constrained to their original self-calibration values. The station parameters were allowed to freely adjust. Three station coordinates and three pointing angles were recovered for each camera at each calibration angle of attack. These parameters were linear functions of angle of attack; hence, the slope-intercept equations were used for computation of the six station parameters for each camera. The recovered station parameters and corresponding computed slope-intercept equation coefficients for both camera stations are summarized in table 4.

Triangulation of results. The coordinates of each wing target for the test data were triangulated with the use of the calibrated camera parameters and the computed station parameters for each tab point. The average value of the estimated rms precision for the resulting Z -coordinates for all tab points was found to be 0.011 inch varying from 0.006 (inboard targets) to 0.015 inch (outboard targets near wingtip). The rotational component of angle of attack was removed from the data, so that wing shape deformations due to aerodynamic loading could be obtained by direct subtraction of triangulated Z -values for corresponding targets given in table 2.

Accuracy of Wind-Tunnel Parameters and Model Angles

Mach Number and Dynamic Pressure

Wind-tunnel flow parameters are obtained by measuring four primary values. They are stagnation pressure p_t , static pressure p_s , stagnation temperature T , and the percent purity of the gas medium from which the ratio of specific heats is obtained. The stagnation and static pressures are measured by two modern laboratory quality pressure gauges. The accuracy of these gauges is 0.02 percent of full scale which is approximately 0.4 psf over the tunnel operation pressure range of 0 to 2200 psf. The values of stagnation temperature and the ratio of specific heats do not vary appreciably during most testing and do not contribute any significant errors to the calculation of flow parameters such as Mach number

M and dynamic pressure q . It is well-known that q is related directly to the value of p_s and that M is a function of the square root of q . Therefore, for most testing in the Langley Transonic Dynamics Tunnel operating envelope, the Mach number is set and held to within 0.002 of the desired value, and the dynamic pressure value is accurate to well within 1.0 psf.

Wing-Root Angle of Attack and Control Surface Angle

The model was instrumented near the wing root with a servo accelerometer and at the inboard side of the control surface shaft with a precision rotary potentiometer. The accuracy of the accelerometer allowed the wing angle of attack to be set to within 0.01° . The control surface angle was accurate to within 0.1° .

Presentation of Results

The results of quasi-steady deflection measurements for an aeroelastic research wing are tabulated in a "Supplement to NASA Technical Memorandum 4194." Representative results from the supplement for a typical test condition are presented in table 5, which shows the spatial coordinates for the wing targets and the corresponding test conditions. In table 5, the spatial coordinate entries which are a series of 9's indicate that the data were not available or were defective. A compilation of quasi-steady test conditions is presented in table 6. The data of table 6 show the tab point, Mach number, dynamic pressure, angle of attack, and outboard control surface deflection angle. A correlation between the graphic and tabulated results is given in table 7. Unless otherwise stated, the tests were conducted in a heavy gas medium (R-12).

A graphical overview of the results in the supplement is presented in figures 6 through 30 as indicated in the following table. Data are presented in figures 6 and 7 to show a comparison of the results obtained from photogrammetric and cathetometric measurements and chordwise deflection of the model at various loadings, respectively. The front and rear spar deflections for variations of angle of attack and outboard control surface deflection are presented in figures 8 through 22. Variations of the spar tip deflection as a function of angle of attack and control surface deflection are presented in figures 23 through 28. Limited data are also presented in figures 29 and 30 to show some effects of dynamic pressure and Mach number on spar tip deflections.

| | Figure |
|---|--------|
| Photogrammetric and cathetometric results for wingtip measurements | 6 |
| Effect of dynamic pressure on wing chordwise deflection at selected rows of targets along the span at $M = 0.850$, $\alpha = 1^\circ$, and $q = 100, 200$, and 300 psf | 7 |
| Variation of wing front and rear spar shapes with angle of attack at four Mach numbers and $q = 100$ psf | 8 |
| Variation of wing front and rear spar shapes with control surface deflection at two angles of attack, $q = 100$ psf, and $M = 0.600$ | 9 |
| Variation of wing front and rear spar shapes with control surface deflection at two angles of attack, $q = 100$ psf, and $M = 0.700$ | 10 |
| Variation of wing front and rear spar shapes with control surface deflection at two angles of attack, $q = 100$ psf, and $M = 0.800$ | 11 |
| Variation of wing front and rear spar shapes with control surface deflection at two angles of attack, $q = 100$ psf, and $M = 0.850$ | 12 |
| Variation of wing front and rear spar shapes with control surface deflection at two angles of attack, $q = 100$ psf, and $M = 0.880$ | 13 |

| | |
|--|----|
| Variation of wing front and rear spar shapes with angle of attack at four Mach numbers and $q = 200$ psf | 14 |
| Variation of wing front and rear spar shapes with control surface deflection at two angles of attack, $q = 200$ psf, and $M = 0.600$ | 15 |
| Variation of wing front and rear spar shapes with control surface deflection at two angles of attack, $q = 200$ psf, and $M = 0.700$ | 16 |
| Variation of wing front and rear spar shapes with control surface deflection at two angles of attack, $q = 200$ psf, and $M = 0.800$ | 17 |
| Variation of wing front and rear spar shapes with control surface deflection at two angles of attack, $q = 200$ psf, and $M = 0.850$ | 18 |
| Variation of wing front and rear spar shapes with angle of attack at $M = 0.800$ and $q = 300$ psf | 19 |
| Variation of wing front and rear spar shapes with control surface deflection at $\alpha = 0^\circ$, $q = 300$ psf, and $M = 0.800$ | 20 |
| Variation of wing front and rear spar shapes with angle of attack at $M = 0.800$ and $q = 100$ psf in air | 21 |
| Variation of wing front and rear spar shapes with control surface deflection at two angles of attack, $q = 100$ psf, and $M = 0.800$ in air | 22 |
| Variation of wing front and rear spar tip deflection with angle of attack at four Mach numbers and $q = 100$ psf | 23 |
| Variation of wing front and rear spar tip deflection with angle of attack at four Mach numbers and $q = 200$ psf | 24 |
| Variation of wing front and rear spar tip deflection with angle of attack at $M = 0.800$ and $q = 300$ psf | 25 |
| Variation of wing front and rear spar tip deflection with control surface deflection at five Mach numbers, two angles of attack, and $q = 100$ psf | 26 |
| Variation of wing front and rear spar tip deflection with control surface deflection at four Mach numbers, two angles of attack, and $q = 200$ psf | 27 |
| Variation of wing front and rear spar tip deflection with control surface deflection at $\alpha = 0^\circ$, $M = 0.800$, and $q = 300$ psf | 28 |
| Variation of average wing spar tip deflection with dynamic pressure at $M = 0.700, 0.800$, and 0.850 and three angles of attack | 29 |
| Variation of average wing spar tip deflection with Mach number at $q = 100$ and 200 psf and three angles of attack | 30 |

Discussion of Results

Photogrammetric data were obtained for the test conditions when the response of the wing to the aerodynamic loading was characterized as either static or quasi-static. Since the photogrammetric technique used in this test program generated instantaneous deflection data, care was taken to avoid recording data when the model tip response was significantly unsteady due to excessive noise, turbulence, flow separation, or other flow phenomena (ref. 11). This unsteady response was the experience for many test conditions at high dynamic pressures and/or Mach numbers. Subsequent to photography, an additional visual deflection measurement was made of the wingtip elevation by use of

a cathetometer. The cathetometric measurements were monitored over a period of about 15 seconds to obtain an average value of the relative wingtip elevation.

Photogrammetric and cathetometric results are graphically presented in figure 6. The photogrammetric results were obtained for measurements of target 1003 which is located midway between the front and rear spars on target row 10. The cathetometric results were obtained from measurements of a line on the wingtip between the projected front and rear spars. A line of agreement and a first-order regression line (least-squares fit) are included with the data as an aid for comparison. The data of figure 6 show that there was good agreement between the photogrammetric and cathetometric techniques. The slope of

the regression line is about 5 to 6 percent lower than that for the line of agreement. This difference is considered to be small and is attributed to the use of nonmetric cameras, the relative location of the target to the wingtip, and the unsteadiness of the model.

Wing Chordwise Bending

Selected data from the photogrammetric results are presented in figure 7 to indicate the chordwise rigidity of the wing at various locations along the span (fig. 3). The data of figure 7 show variations of the net local chordwise deflections normalized by the free-stream dynamic pressure at four different stations. As indicated in the figure, results are presented for three free-stream dynamic pressures at four spanwise stations. The wing deflections are the net measured values (wind-off values removed) normalized by the dynamic pressure for targets located on rows 2, 5, 7, and 9 (fig. 3). Rows 2, 5, and 7 were approximately normal to the wing rear spar, and row 9 was streamwise. The data indicate that the local deflection along the chordwise stations was essentially linear for each row of targets and for each dynamic pressure. The data for the more inboard row of targets (row 2) show a near-zero slope, and small positive slopes are shown for the other rows. Furthermore, the slope of the chordwise deflections became larger as the location of the rows approached the wingtip. The essentially constant slope of the local chordwise deflections for these data indicates that there was sufficient chordwise rigidity of the wing to effectively prevent chordwise bending of the wing model for the range of test conditions.

Wing Spar Deflections

A graphical overview of the photogrammetric wing surface deflection measurements in the heavy gas medium, unless otherwise noted, is presented in the form of plots which show spanwise variations of the vertical deflection (i.e., the vertical spatial coordinate) for the front and rear spars. The results are arranged according to dynamic pressure and Mach number. For increasing Mach number, figures 8 through 13 show deflection data for a dynamic pressure of 100 psf, figures 14 through 18 show deflection data for a dynamic pressure of 200 psf, and figures 19 and 20 show deflection data for 300 psf. Additional deflection data for a dynamic pressure of 100 psf obtained with air as the test medium are shown in figures 21 and 22. Figures 8, 14, 19, and 21 show variations of the wing spar deflections of shapes for various angles of attack and Mach numbers; the remainder of the figures in each group show variations of wing spar deflections for various control surface deflections

at angles of attack of approximately 0° and 2° . The variations of the front and rear spar shapes with angle of attack and control surface deflections (figs. 8 through 22) show the expected characteristic shape typical of a similar cantilever beam. Generally, the spar deflections along the span increased as angle of attack and control surface deflection were increased in the range of test conditions. The expected peak deflections occurred at the spar tips. The influence of control surface deflection on the spar shapes was small compared with that of angle of attack. The influence of control surface deflection in some tests was smaller than that of the unsteady motion of the wing. A typical indication of this condition is shown in figures 13(a) and 13(b) where the magnitude of the vertical deflections does not necessarily increase with control surface deflection (angle of attack of 0° and control surface deflections from -2° to -1° and 4° to 6°).

Variations of the outboard chordwise target vertical positions (targets 1002 and 1004) with angle of attack and control surface deflection are shown in figures 23 through 25 and figures 26 through 28, respectively, for dynamic pressures of 100, 200, and 300 psf. These plots are companion ones of the results in figures 8 through 23 and are generated to show the linearity of the spar tip deflection with angle of attack and control surface deflection. Variations of the spar tip deflection with angle of attack and control surface deflection were somewhat linear for the ranges of test conditions. The scatter in the results for control surface deflection indicates an effect of occasional random deflection errors mentioned in the discussion of figures 8 through 22.

Effect of Dynamic Pressure

The effect of dynamic pressure on the average tip deflection of the two wing spars relative to the wind-off test condition is indicated in the results presented in figure 29. The wingtip deflection was approximated as the average deflection of targets 1002 and 1004. The data show variations of the average tip deflection of the wing spars with dynamic pressure for angles of attack of -1° , 0° , and 1° at Mach numbers of 0.700, 0.800, and 0.850 and with control surface deflection of 0° . The data (fig. 29) show that the wingtip deflection increases with dynamic pressure as it was varied from about 40 to 300 psf. The variations of wingtip deflection with dynamic pressure indicate that for certain conditions, the wingtip deflection may approach maximum or asymptotic values at high dynamic pressures. Such a maximum value of wingtip deflection is indicated for an angle of attack of 1° at Mach numbers of 0.800 and 0.850. Although

dynamic pressure increased wingtip deflection, as expected, this effect was accentuated by increasing the angle of attack.

Effect of Mach Number

The effect of Mach number on the average wing spar tip deflection of the two wing spars relative to the wind-off test condition is indicated in the results presented in figure 30. The data of figure 30 show that for a given Mach number the angle of attack has a significant uniform effect. The data of figure 30 also show that Mach number has an insignificant effect on the wingtip deflection up to a value of about 0.800; above this value, the wingtip deflection may increase or decrease depending on angle of attack. Figure 30(a) for which the dynamic pressure is 100 psf shows that wingtip deflection increased with Mach number regardless of the angle of attack but the trend is inconsistent for the higher dynamic pressure of 200 psf as shown in figure 30(b).

Concluding Remarks

Photogrammetric measurements of the static (quasi-static) wing surface deflections for a flexible aeroelastic supercritical research wing are presented herein. Wing deflection data were obtained at Mach numbers up to 0.900, angles of attack in the range from -2° to 4° , control surface deflections in the range from -8° to 8° , and dynamic pressures in the range from 42 psf to 312 psf.

A comparison of photogrammetric and cathetometric measurements of wingtip deflection shows very good agreement. A graphical overview of the photogrammetric measurements shows significant variations of the wing spars and wingtip vertical deflections. The trends of the variations were quite consistent over the range of test conditions. There were significant variations of wingtip deflection with dynamic pressure that increased with angle of attack. The data indicated the development of a possible maximum or asymptotic value of wingtip deflection in the range of dynamic pressures from about 200 to 300 psf. The effect of Mach number on the wingtip deflection was generally insignificant for Mach numbers up to 0.800. A trend toward larger wingtip deflections was indicated for Mach numbers above 0.800 at the lower dynamic pressure of 100 psf. However, this effect of Mach number at a dynamic pressure of 200 psf was not as consistent.

NASA Langley Research Center
Hampton, VA 23665-5225
September 26, 1990

References

1. Hess, R. W.; Wynne, E. C.; and Cazier, F. W., Jr.: *Static and Unsteady Pressure Measurements on a 50 Degree Clipped Delta Wing at $M = 0.9$* . NASA TM-83297, 1982.
2. Sandford, M. C.; Ricketts, R. H.; Cazier, F. W., Jr.; and Cunningham, H. J.: Transonic Unsteady Airloads on an Energy Efficient Transport Wing With Oscillating Control Surfaces. *J. Aircr.*, vol. 18, no. 7, July 1981, pp. 557-561.
3. Ricketts, Rodney H.; Sandford, Maynard C.; Seidel, David A.; and Watson, Judith J.: Transonic Pressure Distributions on a Rectangular Supercritical Wing Oscillating in Pitch. *J. Aircr.*, vol. 21, no. 8, Aug. 1984, pp. 576-582.
4. Sandford, Maynard C.; Seidel, David A.; Eckstrom, Clinton V.; and Spain, Charles V.: Geometrical and Structural Properties of an Aeroelastic Research Wing. NASA TM-4110, 1989.
5. Seidel, David A.; Sandford, Maynard C.; and Eckstrom, Clinton V.: Measured Unsteady Transonic Aerodynamic Characteristics of an Elastic Supercritical Wing. *J. Aircr.*, vol. 24, no. 4, Apr. 1987, pp. 225-230.
6. Seidel, David A.; Eckstrom, Clinton V.; and Sandford, Maynard C.: Investigation of Transonic Region of High Dynamic Response Encountered on an Elastic Supercritical Wing. *Technical Papers, Part 2A, 28th Structures, Structural Dynamics and Materials Conference and AIAA Dynamics Specialists Conference*, Apr. 1987, pp. 66-75. (Available as AIAA-87-0735.)
7. Byrdson, Thomas A.; and Brooks, Cuyler W., Jr.: *Wind-Tunnel Investigation of Longitudinal and Lateral-Directional Stability and Control Characteristics of a 0.237-Scale Model of a Remotely Piloted Research Vehicle With a Thick, High-Aspect-Ratio Supercritical Wing*. NASA TM-81790, 1980.
8. Reed, Wilmer H., III: *Aeroelasticity Matters: Some Reflections on Two Decades of Testing in the NASA Langley Transonic Dynamics Tunnel*. NASA TM-83210, 1981.
9. Brown, Duane C.: *Application of Close-Range Photogrammetry to Measurements of Structures in Orbit*, Volumes 1 and 2. GSI Tech. Rep. No. 80-012 (Contract No. MOM7DNS-895942), Geodetic Services Inc., Sept. 15, 1980.
10. Brown, Duane C.: STARS (Simultaneous Triangulation And Resection System), A Turnkey System for Close Range Photogrammetry. Presented at Symposium: Precision and Speed in Close Range Photogrammetry (York, England), Sept. 1982.
11. Ross, R.; and Rohne, P. B.: The Character of Flow Unsteadiness and Its Influence on Steady State Transonic Wind Tunnel Measurements. *Windtunnel Design and Testing Techniques*, AGARD-CP-174, 1976, pp. 45-1-45-5.

Table 1. Spatial Coordinates of Target Locations on Wing Lower Surface
in Tunnel Axis System

[All coordinates are in inches]

| Target | x_S | y_S | z_S^a |
|------------------|---------|--------|---------|
| 101 | 256.329 | 40.470 | 57.918 |
| 102 | 259.464 | 39.067 | 57.344 |
| 103 | | | |
| 104 | 267.214 | 35.600 | 57.258 |
| 105 | 271.163 | 33.838 | 57.849 |
| 106 | | | |
| ^b 107 | 276.026 | 31.668 | 58.503 |
| ^b 108 | 278.925 | 30.374 | 58.420 |
| 201 | 262.163 | 51.243 | 57.880 |
| 202 | 265.009 | 49.975 | 57.514 |
| 203 | 268.557 | 48.364 | 57.433 |
| 204 | 272.195 | 46.737 | 57.656 |
| 205 | 274.206 | 45.837 | 57.975 |
| 206 | | | |
| ^b 207 | 278.225 | 44.046 | 58.675 |
| ^b 208 | 280.617 | 42.979 | 58.661 |
| 301 | 277.437 | 50.676 | 58.230 |
| 302 | 280.996 | 49.090 | 58.701 |
| 401 | 268.944 | 63.767 | 57.498 |
| 402 | 271.447 | 62.652 | 57.144 |
| 403 | 274.682 | 61.210 | 57.070 |
| 404 | 277.992 | 59.735 | 57.359 |
| 405 | 280.732 | 58.514 | 57.908 |
| 406 | 284.090 | 57.017 | 58.385 |
| 501 | 275.247 | 75.410 | 56.981 |
| 502 | 277.432 | 74.437 | 56.643 |
| 503 | 280.365 | 73.129 | 56.549 |
| 504 | 283.366 | 71.792 | 56.769 |
| 505 | 285.850 | 70.684 | 57.256 |
| 506 | 288.895 | 69.327 | 57.746 |

| Target | x_S | y_S | z_S^a |
|------------------|---------|---------|---------|
| 601 | 281.550 | 87.052 | 56.333 |
| 602 | 283.416 | 86.221 | 55.995 |
| 603 | 286.047 | 85.048 | 55.883 |
| 604 | 288.740 | 83.848 | 56.046 |
| 605 | 290.969 | 82.855 | 56.457 |
| 606 | 293.700 | 81.637 | 56.942 |
| 701 | 286.899 | 96.930 | 55.662 |
| 702 | 288.494 | 96.220 | 55.328 |
| 703 | 290.869 | 95.161 | 55.210 |
| 704 | 293.299 | 94.078 | 55.320 |
| 705 | | | |
| ^b 706 | 295.752 | 92.949 | 55.752 |
| ^b 707 | 297.777 | 92.082 | 56.132 |
| ^b 801 | 298.505 | 93.948 | 55.977 |
| 901 | 290.781 | 104.389 | 55.335 |
| 902 | 292.589 | 104.283 | 54.757 |
| 903 | 295.192 | 104.228 | 54.569 |
| 904 | 297.821 | 104.223 | 54.574 |
| 905 | | | |
| ^b 906 | 300.521 | 104.223 | 54.860 |
| ^b 907 | 302.447 | 104.047 | 55.137 |
| 1001 | 293.212 | 108.591 | 54.851 |
| 1002 | 294.983 | 108.998 | 54.421 |
| 1003 | 297.466 | 108.998 | 54.229 |
| 1004 | 299.949 | 108.998 | 54.215 |
| 1005 | 301.963 | 108.998 | 54.393 |
| 1006 | 304.379 | 108.998 | 54.721 |

^aEstimated lg value.

^bTargets on control surfaces.

Table 2. Corrected Spatial Coordinates of Target Locations on Wing Lower Surface

[All coordinates are in inches]

| Target | X _S | Y _S | Z _S | Target | X _S | Y _S | Z _S |
|------------------|----------------|----------------|----------------|-------------------|----------------|----------------|----------------|
| 101 | 255.480 | 40.507 | 60.904 | 601 | 280.511 | 86.830 | 59.042 |
| ^a 102 | 258.641 | 39.109 | 60.405 | 602 | 282.378 | 86.000 | 58.876 |
| ^b 103 | 263.393 | 37.023 | 60.219 | 603 | 285.043 | 84.908 | 58.860 |
| 104 | 266.405 | 35.675 | 60.416 | 604 | 287.754 | 83.792 | 59.160 |
| ^a 105 | 270.375 | 33.867 | 61.022 | 605 | 290.036 | 82.900 | 59.636 |
| ^b 106 | 273.771 | 32.321 | 61.522 | 606 | 292.784 | 81.788 | 59.855 |
| ^c 107 | 275.159 | 31.670 | 61.603 | | | | |
| ^c 108 | 278.070 | 30.395 | 61.426 | 701 | 285.837 | 96.627 | 58.307 |
| | | | | 702 | 287.423 | 95.987 | 58.176 |
| 201 | 261.293 | 51.310 | 60.836 | 703 | 289.839 | 94.966 | 58.180 |
| 202 | 264.164 | 50.026 | 60.542 | 704 | 292.349 | 93.948 | 58.433 |
| 203 | 267.699 | 48.446 | 60.498 | ^b 705 | 293.855 | 93.289 | 58.728 |
| 204 | 271.458 | 46.783 | 60.875 | ^c 706 | 294.798 | 92.960 | 58.950 |
| 205 | 273.309 | 45.940 | 61.215 | ^c 707 | 296.868 | 92.049 | 59.087 |
| ^b 206 | 275.933 | 44.899 | 61.660 | | | | |
| ^c 207 | 277.303 | 44.193 | 61.779 | ^c 801 | 297.586 | 93.930 | 58.939 |
| ^c 208 | 279.696 | 43.157 | 61.643 | | | | |
| | | | | 901 | 289.789 | 104.190 | 57.731 |
| 301 | 276.578 | 50.746 | 61.426 | 902 | 291.532 | 104.166 | 57.585 |
| 302 | 280.062 | 49.179 | 61.731 | 903 | 294.148 | 104.105 | 57.508 |
| | | | | 904 | 296.757 | 104.107 | 57.664 |
| 401 | 268.018 | 63.769 | 60.389 | ^b 905 | 298.466 | 104.123 | 57.935 |
| 402 | 270.484 | 62.676 | 60.146 | ^c 906 | 299.395 | 104.037 | 58.055 |
| 403 | 273.738 | 61.239 | 60.117 | ^c 907 | 301.383 | 104.008 | 58.155 |
| 404 | 277.094 | 59.807 | 60.508 | | | | |
| 405 | 279.825 | 58.581 | 61.084 | 1001 | 292.293 | 108.825 | 57.365 |
| 406 | 283.171 | 57.127 | 61.351 | 1002 | 293.871 | 108.790 | 57.214 |
| | | | | ^a 1003 | 296.405 | 108.831 | 57.160 |
| 501 | 274.348 | 75.278 | 59.773 | 1004 | 298.799 | 108.910 | 57.284 |
| 502 | 276.475 | 74.365 | 59.576 | 1005 | 300.827 | 108.929 | 57.583 |
| 503 | 279.417 | 73.080 | 59.574 | 1006 | 303.276 | 108.856 | 57.676 |
| 504 | 282.389 | 71.785 | 59.903 | | | | |
| 505 | 284.929 | 70.699 | 60.443 | | | | |
| 506 | 287.970 | 69.400 | 60.683 | | | | |

^aBundle adjustment control points.

^bTargets added after self-calibration.

^cTargets located on control surfaces.

Table 3. rms Estimated Measurement Precision for Target Spatial Coordinates

[All coordinates are in inches]

| Target | X _S , rms | Y _S , rms | Z _S , rms |
|--------|----------------------|----------------------|----------------------|
| 101 | 0.0045 | 0.0050 | 0.0048 |
| a102 | | | |
| b103 | | | |
| 104 | 0.0030 | 0.0037 | 0.0035 |
| a105 | | | |
| b106 | | | |
| c107 | 0.0041 | 0.0051 | 0.0049 |
| c108 | 0.0049 | 0.0060 | 0.0059 |
| 201 | 0.0059 | 0.0061 | 0.0046 |
| 202 | 0.0055 | 0.0056 | 0.0040 |
| 203 | 0.0052 | 0.0052 | 0.0036 |
| 204 | 0.0052 | 0.0052 | 0.0035 |
| 205 | 0.0053 | 0.0053 | 0.0037 |
| b206 | | | |
| c207 | 0.0057 | 0.0058 | 0.0043 |
| c208 | 0.0061 | 0.0062 | 0.0049 |
| 301 | 0.0071 | 0.0067 | 0.0039 |
| 302 | 0.0074 | 0.0071 | 0.0044 |
| 401 | 0.0098 | 0.0094 | 0.0047 |
| 402 | 0.0096 | 0.0092 | 0.0042 |
| 403 | 0.0096 | 0.0090 | 0.0039 |
| 404 | 0.0096 | 0.0090 | 0.0038 |
| 405 | 0.0098 | 0.0090 | 0.0040 |
| 406 | 0.0101 | 0.0093 | 0.0045 |
| 501 | 0.0139 | 0.0131 | 0.0046 |
| 502 | 0.0139 | 0.0130 | 0.0042 |
| 503 | 0.0139 | 0.0129 | 0.0039 |
| 504 | 0.0139 | 0.0129 | 0.0039 |
| 505 | 0.0141 | 0.0129 | 0.0041 |
| 506 | 0.0143 | 0.0131 | 0.0046 |

| Target | X _S , rms | Y _S , rms | Z _S , rms |
|--------|----------------------|----------------------|----------------------|
| 601 | 0.0182 | 0.0170 | 0.0046 |
| 602 | 0.0182 | 0.0170 | 0.0043 |
| 603 | 0.0183 | 0.0169 | 0.0041 |
| 604 | 0.0183 | 0.0169 | 0.0041 |
| 605 | 0.0185 | 0.0170 | 0.0043 |
| 606 | 0.0187 | 0.0171 | 0.0046 |
| 701 | 0.0220 | 0.0205 | 0.0046 |
| 702 | 0.0220 | 0.0205 | 0.0044 |
| 703 | 0.0220 | 0.0205 | 0.0042 |
| 704 | 0.0221 | 0.0205 | 0.0043 |
| b705 | | | |
| c706 | 0.0222 | 0.0205 | 0.0045 |
| c707 | 0.0223 | 0.0206 | 0.0048 |
| c801 | 0.0229 | 0.0212 | 0.0048 |
| 901 | 0.0248 | 0.0233 | 0.0048 |
| 902 | 0.0250 | 0.0234 | 0.0046 |
| 903 | 0.0254 | 0.0237 | 0.0046 |
| 904 | 0.0257 | 0.0241 | 0.0047 |
| b905 | | | |
| c906 | 0.0261 | 0.0244 | 0.0049 |
| c907 | 0.0265 | 0.0247 | 0.0052 |
| 1001 | 0.0265 | 0.0249 | 0.0048 |
| 1002 | 0.0267 | 0.0251 | 0.0047 |
| a1003 | 0.0271 | 0.0254 | |
| 1004 | 0.0275 | 0.0257 | 0.0048 |
| 1005 | 0.0278 | 0.0260 | 0.0050 |
| 1006 | 0.0282 | 0.0263 | 0.0054 |

- a Bundle adjustment control points
 b Targets added after self-calibration
 c Targets located on control surfaces

Table 4. Summary of Angle-of-Attack Calibration Results

| Station parameters | Angle of attack, deg | | | | | | | Least-squares results | | |
|--------------------------|----------------------|----------|----------|----------|----------|----------|----------|-----------------------|----------|-----------|
| | -2.0288 | -1.0150 | -0.0612 | 1.0349 | 2.0357 | 3.0510 | 4.0271 | a_1 | a_0 | C_{cor} |
| Forward camera station | | | | | | | | | | |
| x_c , in. | 261.1423 | 261.6075 | 262.0370 | 262.5255 | 262.9913 | 263.4311 | 263.8687 | 0.4508 | 262.0582 | 0.9999 |
| y_c , in. | -3.5917 | -3.6370 | -3.6448 | -3.6088 | -3.6057 | -3.6202 | -3.5936 | 0.0024 | -3.6169 | 0.2531 |
| z_c , in. | 31.5574 | 31.6652 | 31.8048 | 31.9645 | 32.0994 | 32.2561 | 32.4258 | 0.1439 | 31.8218 | 0.9983 |
| ψ , deg | 2.1495 | 1.8100 | 1.4963 | 1.1327 | 0.7821 | 0.4519 | 0.1127 | -0.3365 | 1.4744 | -0.9999 |
| θ , deg | 18.6309 | 18.6742 | 18.6824 | 18.7162 | 18.7417 | 18.7462 | 18.7567 | 0.0205 | 18.6861 | 0.9722 |
| ϕ , deg | 1.8746 | 0.8324 | -0.2070 | -1.3443 | -2.4020 | -3.4500 | -4.5027 | -1.0543 | -0.2464 | -0.9999 |
| Aft camera station | | | | | | | | | | |
| x_c , in. | 302.9109 | 303.3734 | 303.7989 | 304.2812 | 304.7209 | 305.0942 | 305.5056 | 0.4286 | 303.8065 | 0.9996 |
| y_c , in. | -6.3497 | -6.3765 | -6.3773 | -6.3815 | -6.3901 | -6.4246 | -6.4043 | -0.0096 | -6.3766 | -0.8918 |
| z_c , in. | 30.6329 | 31.5041 | 32.3214 | 33.2495 | 34.1697 | 35.0182 | 35.9238 | 0.8729 | 32.3759 | 0.9999 |
| ψ , deg | -25.6405 | -25.8889 | -26.1203 | -26.3855 | -26.6297 | -26.8240 | -27.0622 | -0.2344 | -26.1271 | -0.9995 |
| θ , deg | 16.1339 | 15.6699 | 15.2693 | 14.7995 | 14.3135 | 13.8911 | -13.4282 | -0.4455 | 15.2376 | -0.9998 |
| ϕ , deg | 3.4554 | 2.4625 | 1.6067 | 0.5936 | -0.3706 | -1.2651 | -2.1730 | -0.9283 | 1.5557 | -0.9999 |

Table 5. Wing Deflection Measurements for Typical Test Condition

$$\left[\begin{array}{l} \text{Tab point} = 108; M = 0.791; q = 99.796 \text{ psf;} \\ \alpha = 1.024^\circ; \delta = -0.065^\circ \end{array} \right]$$

| Target | X _S | Y _S | Z _S | Target | X _S | Y _S | Z _S |
|------------------|----------------|----------------|----------------|--------|----------------|----------------|----------------|
| 101 | 255.507 | 40.399 | 61.101 | 601 | 280.601 | 86.709 | 60.884 |
| 102 | 258.669 | 39.017 | 60.611 | 602 | 282.459 | 85.984 | 60.757 |
| 103 | 263.414 | 36.919 | 60.407 | 603 | 285.125 | 84.866 | 60.748 |
| 104 | 266.430 | 35.572 | 60.600 | 604 | 287.832 | 83.751 | 61.053 |
| 105 | 270.391 | 33.785 | 61.228 | 605 | 290.118 | 82.855 | 61.555 |
| 106 | 273.797 | 32.220 | 61.721 | 606 | 292.859 | 81.695 | 61.762 |
| ^a 107 | 999.999 | 99.999 | 99.999 | 701 | 285.930 | 96.652 | 60.723 |
| ^a 108 | 999.999 | 99.999 | 99.999 | 702 | 287.524 | 95.949 | 60.596 |
| 201 | 261.330 | 51.190 | 61.243 | 703 | 289.938 | 94.922 | 60.606 |
| 202 | 264.206 | 49.886 | 60.926 | 704 | 292.442 | 93.942 | 60.897 |
| 203 | 267.731 | 48.321 | 60.898 | 705 | 293.951 | 93.239 | 61.187 |
| 204 | 271.484 | 46.664 | 61.283 | 706 | 294.872 | 92.862 | 61.394 |
| 205 | 273.344 | 45.790 | 61.585 | 707 | 296.979 | 91.987 | 61.554 |
| 206 | 275.962 | 44.755 | 62.038 | 801 | 297.688 | 93.904 | 61.516 |
| 207 | 277.329 | 44.073 | 62.175 | 901 | 289.890 | 104.200 | 60.605 |
| 208 | 279.721 | 43.017 | 62.027 | 902 | 291.641 | 104.103 | 60.476 |
| 301 | 276.610 | 50.607 | 61.944 | 903 | 294.265 | 104.054 | 60.477 |
| 302 | 280.091 | 49.062 | 62.267 | 904 | 296.865 | 104.061 | 60.679 |
| 401 | 268.076 | 63.628 | 61.162 | 905 | 298.585 | 104.060 | 60.994 |
| 402 | 270.534 | 62.555 | 60.923 | 906 | 299.510 | 104.073 | 61.166 |
| 403 | 273.780 | 61.153 | 60.901 | 907 | 301.487 | 103.952 | 61.284 |
| 404 | 277.129 | 59.690 | 61.286 | 1001 | 292.418 | 108.764 | 60.477 |
| 405 | 279.869 | 58.452 | 61.858 | 1002 | 293.993 | 108.936 | 60.432 |
| 406 | 283.213 | 57.026 | 62.154 | 1003 | 296.534 | 108.821 | 60.392 |
| 501 | 274.405 | 75.226 | 61.061 | 1004 | 298.928 | 108.992 | 60.611 |
| 502 | 276.539 | 74.284 | 60.858 | 1005 | 300.927 | 108.892 | 60.944 |
| 503 | 279.487 | 72.953 | 60.849 | 1006 | 303.378 | 108.830 | 61.088 |
| 504 | 282.456 | 71.716 | 61.210 | | | | |
| 505 | 284.981 | 70.622 | 61.751 | | | | |
| 506 | 288.029 | 69.277 | 61.986 | | | | |

^aTarget spatial coordinates were not available.

Table 6. Quasi-Steady Test Conditions for Wing Deflection Measurements

| Tab point | M | q, psf | α , deg | δ , deg | Remarks |
|-----------|-------|-----------|-------------------|-------------------|---------------------|
| 001 | 0.000 | 0.000 | 0.000 | 0.000 | Wind-off zero |
| 210 | 0.600 | 100.518 | -2.014 | 0.008 | α sweep ↓ |
| 211 | 0.600 | 99.982 | -1.029 | -0.044 | |
| 212 | 0.600 | 100.400 | 0.023 | -0.019 | |
| 213 | 0.600 | 99.805 | 1.019 | 0.006 | |
| 214 | 0.600 | 101.192 | 2.027 | -0.018 | |
| 215 | 0.600 | 100.599 | 3.005 | -0.013 | |
| 216 | 0.600 | 100.457 | 4.024 | -0.009 | |
| 217 | 0.600 | 100.913 | 0.006 | -7.979 | δ sweep ↓ |
| 218 | 0.600 | 102.756 | 0.006 | -6.003 | |
| 219 | 0.600 | 101.851 | 0.004 | -3.996 | |
| 220 | 0.600 | 100.887 | 0.005 | -3.031 | |
| 221 | 0.600 | 101.218 | 0.005 | -2.051 | |
| 222 | 0.600 | 100.827 | 0.004 | -1.006 | |
| 223 | 0.600 | 99.957 | 0.004 | -0.052 | |
| 224 | 0.600 | 101.487 | 0.004 | 1.001 | |
| 225 | 0.600 | 101.037 | 0.003 | 2.010 | |
| 226 | 0.600 | 101.390 | 0.003 | 3.001 | |
| 227 | 0.600 | 101.434 | 0.004 | 4.020 | |
| 228 | 0.600 | 101.204 | 0.003 | 5.983 | |
| 229 | 0.600 | 101.354 | 0.002 | 8.021 | |
| 230 | 0.600 | 101.028 | 2.000 | -8.034 | δ sweep ↓ |
| 231 | 0.600 | 100.636 | 1.999 | -5.963 | |
| 232 | 0.600 | 100.864 | 2.000 | -4.042 | |
| 233 | 0.600 | 101.678 | 1.999 | -2.991 | |
| 234 | 0.600 | 101.097 | 1.999 | -1.966 | |
| 235 | 0.600 | 101.137 | 1.999 | -1.003 | |
| 236 | 0.600 | 100.625 | 1.999 | 0.050 | |
| 237 | 0.600 | 100.979 | 1.999 | 1.042 | |
| 238 | 0.600 | 100.829 | 2.000 | 2.034 | |
| 239 | 0.600 | 100.958 | 1.999 | 3.027 | |
| 240 | 0.600 | 100.956 | 1.999 | 4.031 | |
| 241 | 0.600 | 100.381 | 1.999 | 6.042 | |
| 242 | 0.600 | 101.127 | 1.998 | 8.059 | |
| 148 | 0.700 | 99.441 | -2.022 | -0.083 | α sweep ↓ |
| 149 | 0.700 | 99.366 | -1.023 | -0.032 | |
| 150 | 0.700 | 100.149 | -0.027 | -0.073 | |
| 151 | 0.700 | 100.003 | 0.997 | -0.004 | |
| 152 | 0.700 | 100.488 | 2.005 | -0.045 | |
| 153 | 0.700 | 99.594 | 2.998 | -0.069 | |
| 154 | 0.700 | 100.195 | 4.024 | -0.066 | |

Table 6. Continued

| Tab Point | M | q, psf | α , deg | δ , deg | Remarks |
|-----------|-------|-----------|-------------------|-------------------|---------------------|
| 168 | 0.700 | 100.240 | -0.008 | -8.026 | δ sweep ↓ |
| 170 | 0.700 | 99.800 | -0.009 | -4.033 | |
| 172 | 0.700 | 100.371 | -0.010 | -2.027 | |
| 176 | 0.700 | 100.680 | -0.010 | 2.017 | |
| 179 | 0.700 | 100.112 | -0.010 | 3.990 | |
| 181 | 0.700 | 100.517 | -0.011 | 8.022 | |
| 155 | 0.700 | 100.361 | 2.009 | -8.014 | δ sweep ↓ |
| 156 | 0.700 | 100.978 | 2.009 | -5.994 | |
| 157 | 0.700 | 100.284 | 2.009 | -4.012 | |
| 159 | 0.700 | 100.092 | 2.009 | -1.985 | |
| 161 | 0.700 | 100.121 | 2.009 | 0.021 | |
| 163 | 0.700 | 100.375 | 2.009 | 2.011 | |
| 165 | 0.700 | 99.718 | 2.008 | 4.037 | α sweep ↓ |
| 80 | 0.800 | 100.879 | -2.003 | -0.028 | |
| 81 | 0.800 | 100.473 | -1.023 | -0.050 | |
| 82 | 0.800 | 100.828 | 0.000 | -0.039 | |
| 108 | 0.800 | 99.796 | 1.024 | -0.065 | |
| 109 | 0.800 | 99.854 | 2.009 | -0.063 | |
| 110 | 0.800 | 100.537 | 2.992 | -0.063 | δ sweep ↓ |
| 111 | 0.800 | 101.735 | 3.998 | -0.064 | |
| 105 | 0.800 | 101.206 | 0.002 | -8.001 | |
| 106 | 0.800 | 100.103 | 0.001 | -5.990 | |
| 107 | 0.800 | 99.419 | 0.001 | -4.075 | |
| 86 | 0.800 | 100.395 | 0.001 | -3.045 | |
| 87 | 0.800 | 101.471 | 0.000 | -2.040 | δ sweep ↓ |
| 88 | 0.800 | 99.910 | 0.000 | -1.045 | |
| 90 | 0.800 | 100.106 | -0.001 | 1.021 | |
| 91 | 0.800 | 100.268 | 0.000 | 1.984 | |
| 92 | 0.800 | 99.694 | 0.000 | 3.043 | |
| 94 | 0.800 | 100.093 | -0.001 | 4.063 | |
| 95 | 0.800 | 98.901 | -0.001 | 6.018 | δ sweep ↓ |
| 96 | 0.800 | 100.250 | -0.001 | 8.053 | |
| 115 | 0.800 | 101.305 | 2.009 | -8.032 | |
| 116 | 0.800 | 101.868 | 2.011 | -6.025 | |
| 117 | 0.800 | 101.968 | 2.010 | -4.027 | |
| 118 | 0.800 | 101.803 | 2.010 | -2.981 | |
| 119 | 0.800 | 102.238 | 2.009 | -2.030 | δ sweep ↓ |
| 120 | 0.800 | 102.029 | 2.009 | -1.035 | |
| 122 | 0.800 | 101.450 | 2.018 | 0.002 | |
| 123 | 0.800 | 101.049 | 2.018 | 1.026 | |
| 124 | 0.800 | 102.573 | 2.018 | 2.014 | |
| 125 | 0.800 | 102.273 | 2.018 | 3.020 | |

Table 6. Continued

| Tab Point | M | q, psf | α , deg | δ , deg | Remarks |
|-----------|-------|-----------|-------------------|-------------------|----------------|
| 126 | 0.800 | 101.966 | 2.018 | 4.004 | δ sweep |
| 127 | 0.800 | 102.336 | 2.018 | 6.011 | ↓ |
| 128 | 0.800 | 101.803 | 2.018 | 8.027 | |
| 783 | 0.850 | 99.778 | -2.008 | 0.033 | α sweep |
| 784 | 0.850 | 99.555 | -1.019 | 0.026 | ↓ |
| 785 | 0.850 | 99.731 | -0.003 | 0.013 | |
| 788 | 0.850 | 100.169 | 1.020 | 0.011 | |
| 789 | 0.850 | 100.344 | 1.998 | 0.025 | |
| 790 | 0.850 | 100.099 | 2.992 | 0.007 | |
| 791 | 0.850 | 100.160 | 4.027 | 0.000 | ↓ |
| 801 | 0.850 | 100.293 | -0.001 | -3.043 | δ sweep |
| 802 | 0.850 | 100.137 | 0.000 | -1.993 | ↓ |
| 803 | 0.850 | 100.860 | -0.001 | -1.037 | |
| 804 | 0.850 | 100.341 | -0.001 | 1.031 | |
| 805 | 0.850 | 100.564 | -0.001 | 2.003 | |
| 806 | 0.850 | 100.618 | -0.001 | 3.021 | |
| 807 | 0.850 | 100.339 | -0.001 | 6.041 | ↓ |
| 792 | 0.850 | 100.435 | 2.021 | -6.068 | δ sweep |
| 793 | 0.850 | 100.334 | 2.020 | -2.998 | ↓ |
| 794 | 0.850 | 100.743 | 2.020 | -1.996 | |
| 795 | 0.850 | 100.994 | 2.021 | -1.031 | |
| 796 | 0.850 | 100.334 | 2.020 | 0.993 | |
| 797 | 0.850 | 100.735 | 2.019 | 2.057 | |
| 798 | 0.850 | 100.396 | 2.019 | 3.057 | |
| 799 | 0.850 | 100.588 | 2.019 | 6.011 | ↓ |
| 268 | 0.880 | 100.628 | -0.023 | -7.998 | δ sweep |
| 270 | 0.880 | 100.401 | -0.023 | -4.003 | ↓ |
| 272 | 0.880 | 100.143 | -0.023 | -2.981 | |
| 273 | 0.880 | 100.873 | -0.024 | -1.996 | |
| 274 | 0.880 | 100.538 | -0.024 | -1.037 | |
| 276 | 0.880 | 100.771 | -0.024 | 1.027 | |
| 277 | 0.880 | 100.642 | -0.024 | 2.032 | |
| 278 | 0.880 | 100.265 | -0.024 | 2.993 | |
| 280 | 0.880 | 101.182 | -0.024 | 3.998 | |
| 281 | 0.880 | 101.251 | -0.024 | 6.026 | ↓ |
| 283 | 0.880 | 101.093 | 2.025 | -4.004 | δ sweep |
| 284 | 0.880 | 99.964 | 2.026 | -3.004 | ↓ |
| 285 | 0.880 | 99.799 | 2.024 | -1.983 | |
| 286 | 0.880 | 100.577 | 2.024 | -1.003 | |
| 287 | 0.880 | 101.147 | 2.024 | 1.011 | |
| 288 | 0.880 | 101.228 | 2.023 | 2.071 | |
| 289 | 0.880 | 101.516 | 2.024 | 2.988 | ↓ |

Table 6. Continued

| Tab Point | M | q, psf | α , deg | δ , deg | Remarks |
|-----------|-------|-----------|-------------------|-------------------|---------------------|
| 290 | 0.880 | 101.144 | 2.024 | 3.987 | δ sweep ↓ |
| 291 | 0.880 | 101.085 | 2.023 | 6.002 | |
| 292 | 0.880 | 101.167 | 2.023 | 7.987 | |
| 293 | 0.880 | 100.972 | 2.024 | 0.048 | |
| 476 | 0.600 | 200.356 | -2.032 | -0.052 | α sweep ↓ |
| 477 | 0.600 | 199.231 | -1.018 | -0.025 | |
| 479 | 0.600 | 199.838 | 1.006 | -0.014 | |
| 481 | 0.600 | 200.093 | 2.011 | -0.035 | |
| 548 | 0.600 | 200.334 | 0.008 | -5.990 | δ sweep ↓ |
| 567 | 0.600 | 202.296 | -0.021 | -1.984 | |
| 568 | 0.600 | 202.321 | -0.023 | -1.010 | |
| 570 | 0.600 | 202.380 | -0.023 | 1.077 | |
| 572 | 0.600 | 203.313 | -0.023 | 2.030 | |
| 573 | 0.600 | 203.768 | -0.023 | 3.050 | |
| 574 | 0.600 | 203.612 | -0.025 | 5.972 | |
| 482 | 0.600 | 199.566 | 2.021 | -5.994 | |
| 483 | 0.600 | 200.161 | 2.020 | -2.987 | δ sweep ↓ |
| 484 | 0.600 | 199.282 | 2.019 | -2.019 | |
| 485 | 0.600 | 200.379 | 2.019 | -1.055 | |
| 486 | 0.600 | 199.522 | 2.019 | 1.048 | |
| 487 | 0.600 | 198.999 | 2.018 | 2.027 | |
| 446 | 0.700 | 200.791 | -2.012 | -0.048 | |
| 449 | 0.700 | 200.373 | -1.032 | -0.052 | α sweep ↓ |
| 450 | 0.700 | 199.582 | 0.015 | -0.060 | |
| 451 | 0.700 | 200.345 | 1.021 | -0.056 | |
| 452 | 0.700 | 200.136 | 2.004 | -0.050 | |
| 465 | 0.700 | 199.957 | -0.014 | -6.015 | |
| 466 | 0.700 | 200.971 | 0.008 | -3.023 | δ sweep ↓ |
| 467 | 0.700 | 199.635 | 0.006 | -2.008 | |
| 468 | 0.700 | 201.693 | 0.006 | -1.041 | |
| 469 | 0.700 | 201.081 | 0.006 | 1.037 | |
| 471 | 0.700 | 200.462 | 0.005 | 2.002 | |
| 473 | 0.700 | 201.172 | 0.005 | 3.032 | |
| 474 | 0.700 | 200.870 | 0.004 | 6.024 | |
| 453 | 0.700 | 199.792 | 2.006 | -6.018 | |
| 455 | 0.700 | 201.403 | 2.005 | -3.030 | |
| 456 | 0.700 | 201.251 | 2.005 | -2.029 | δ sweep ↓ |
| 459 | 0.700 | 199.607 | 2.029 | 1.027 | |
| 460 | 0.700 | 200.688 | 2.028 | 2.030 | |
| 461 | 0.700 | 200.384 | 2.028 | 3.011 | |
| 462 | 0.700 | 200.494 | 2.028 | 6.008 | |
| | | | | | |

Table 6. Continued

| Tab Point | M | q, psf | α , deg | δ , deg | Remarks |
|-----------|-------|-----------|-------------------|-------------------|---------------------|
| 423 | 0.800 | 200.865 | -2.029 | -0.055 | α sweep ↓ |
| 424 | 0.800 | 199.907 | -1.030 | -0.037 | |
| 425 | 0.800 | 201.393 | 0.001 | -0.024 | |
| 426 | 0.800 | 200.616 | 1.026 | -0.035 | |
| 427 | 0.800 | 200.337 | 2.024 | -0.028 | |
| 437 | 0.800 | 204.280 | 0.011 | -6.032 | δ sweep ↓ |
| 438 | 0.800 | 203.288 | 0.011 | -2.994 | |
| 439 | 0.800 | 203.492 | 0.010 | -2.008 | |
| 440 | 0.800 | 202.202 | 0.010 | -1.007 | |
| 441 | 0.800 | 201.853 | 0.009 | 1.015 | |
| 442 | 0.800 | 204.732 | 0.010 | 2.012 | |
| 443 | 0.800 | 203.387 | 0.010 | 3.030 | |
| 444 | 0.800 | 204.540 | 0.009 | 6.036 | |
| 428 | 0.800 | 202.119 | 2.024 | -5.963 | δ sweep ↓ |
| 429 | 0.800 | 201.354 | 2.024 | -3.042 | |
| 431 | 0.800 | 202.829 | 2.024 | -2.024 | |
| 432 | 0.800 | 199.750 | 2.023 | -1.065 | |
| 433 | 0.800 | 201.244 | 2.023 | 1.023 | |
| 434 | 0.800 | 200.533 | 2.024 | 2.032 | |
| 435 | 0.800 | 203.957 | 2.021 | 3.064 | |
| 436 | 0.800 | 203.772 | 2.022 | 6.042 | |
| 911 | 0.850 | 199.727 | -2.022 | -0.048 | α sweep ↓ |
| 912 | 0.850 | 200.654 | -1.032 | -0.039 | |
| 913 | 0.850 | 200.556 | 0.006 | -0.068 | |
| 914 | 0.850 | 200.871 | 1.005 | -0.070 | |
| 915 | 0.850 | 202.492 | 2.021 | -0.065 | |
| 916 | 0.850 | 202.039 | -0.011 | -6.062 | δ sweep ↓ |
| 917 | 0.850 | 200.945 | -0.012 | -3.019 | |
| 918 | 0.850 | 201.597 | -0.013 | -2.009 | |
| 919 | 0.850 | 200.681 | -0.013 | -1.021 | |
| 920 | 0.850 | 202.207 | -0.013 | 1.037 | |
| 921 | 0.850 | 200.895 | -0.014 | 2.024 | |
| 922 | 0.850 | 199.740 | -0.014 | 3.015 | |
| 923 | 0.850 | 203.088 | -0.014 | 5.999 | |
| 924 | 0.850 | 202.528 | 2.020 | -6.007 | δ sweep ↓ |
| 925 | 0.850 | 202.815 | 2.019 | -3.024 | |
| 926 | 0.850 | 200.509 | 2.020 | -2.033 | |
| 927 | 0.850 | 202.695 | 2.020 | -1.010 | |
| 928 | 0.850 | 202.545 | 2.019 | 1.056 | |
| 929 | 0.850 | 200.369 | 2.019 | 2.020 | |
| 930 | 0.850 | 204.826 | 2.020 | 3.067 | |

Table 6. Continued

| Tab Point | M | q, psf | α , deg | δ , deg | Remarks |
|-----------|-------|-----------|-------------------|-------------------|----------------------------------|
| 931 | 0.850 | 202.482 | 2.019 | 5.979 | δ sweep ↓ |
| 932 | 0.850 | 202.730 | 2.019 | 0.056 | |
| 948 | 0.800 | 299.589 | -1.036 | 0.029 | α sweep ↓ |
| 951 | 0.800 | 297.697 | 0.000 | -0.048 | |
| 952 | 0.800 | 298.743 | 1.024 | -0.044 | δ sweep ↓ |
| 953 | 0.800 | 297.301 | 0.006 | -3.005 | |
| 955 | 0.800 | 299.726 | 0.015 | -1.928 | δ sweep ↓ |
| 957 | 0.800 | 295.817 | 0.014 | -0.892 | |
| 958 | 0.800 | 298.955 | 0.011 | 2.993 | δ sweep ↓ |
| 959 | 0.800 | 297.900 | 0.012 | 2.067 | |
| 960 | 0.800 | 298.602 | 0.011 | 0.964 | δ sweep ↓ |
| 961 | 0.800 | 300.477 | 0.011 | 6.090 | |
| 977 | 0.800 | 103.502 | -2.022 | -0.072 | α sweep in air ↓ |
| 978 | 0.800 | 102.518 | -1.019 | 0.049 | |
| 979 | 0.800 | 102.772 | -0.009 | -0.034 | α sweep in air ↓ |
| 980 | 0.800 | 102.729 | 1.009 | -0.033 | |
| 981 | 0.800 | 102.983 | 2.017 | -0.025 | α sweep in air ↓ |
| 982 | 0.800 | 103.579 | 2.968 | -0.029 | |
| 983 | 0.800 | 103.658 | 3.996 | -0.051 | δ sweep in air ↓ |
| 1004 | 0.800 | 104.793 | 0.006 | -6.004 | |
| 1005 | 0.800 | 104.693 | 0.005 | -3.039 | δ sweep in air ↓ |
| 1006 | 0.800 | 104.757 | 0.005 | -2.026 | |
| 1007 | 0.800 | 104.682 | 0.005 | -1.036 | δ sweep in air ↓ |
| 1008 | 0.800 | 104.854 | 0.004 | 1.019 | |
| 1009 | 0.800 | 105.420 | 0.004 | 2.001 | δ sweep in air ↓ |
| 1010 | 0.800 | 105.108 | 0.004 | 2.975 | |
| 1011 | 0.800 | 105.001 | 0.004 | 6.016 | δ sweep in air ↓ |
| 1012 | 0.800 | 105.217 | 2.015 | -6.020 | |
| 1013 | 0.800 | 105.121 | 2.015 | -3.006 | δ sweep in air ↓ |
| 1014 | 0.800 | 105.293 | 2.015 | -2.039 | |
| 1015 | 0.800 | 105.501 | 2.014 | -1.008 | δ sweep in air ↓ |
| 1016 | 0.800 | 105.530 | 2.015 | 1.013 | |
| 1018 | 0.800 | 105.611 | 2.014 | 2.004 | δ sweep in air ↓ |
| 1019 | 0.800 | 105.743 | 2.013 | 3.010 | |
| 1020 | 0.800 | 105.720 | 2.012 | 6.004 | Transition strips installed ↓ |
| 665 | 0.700 | 100.443 | -0.012 | -0.013 | |
| 667 | 0.750 | 111.908 | -0.014 | -0.021 | Transition strips installed ↓ |
| 669 | 0.800 | 123.682 | -0.016 | -0.020 | |
| 671 | 0.850 | 135.351 | -0.017 | -0.030 | Transition strips installed ↓ |
| 673 | 0.870 | 139.763 | -0.018 | -0.022 | |

Table 6. Concluded


| Tab Point | M | q, psf | α , deg | δ , deg | Remarks |
|-----------|-------|-----------|-------------------|-------------------|---|
| 680 | 0.700 | 100.216 | -0.010 | -0.044 | Air data  |
| 685 | 0.750 | 111.773 | -0.015 | -0.034 | |
| 689 | 0.800 | 123.632 | -0.013 | -0.047 | |
| 691 | 0.850 | 133.431 | -0.015 | -0.043 | |

Table 7. Correlation of Graphic and Tabulated Results

| Figure (a) | Tab point |
|---------------|--|
| | Angle-of-attack variation: |
| 8(aT) | 001, 211, 212, 213, 214, 215, 216 |
| 8(bT) | 001, 148, 149, 150, 151, 152, 153, 154 |
| 8(cT) | 001, 80, 81, 82, 108, 109, 110, 111 |
| 8(dT) | 001, 783, 784, 785, 788, 789, 790, 791 |
| | Control surface deflection variation: |
| 9(aT) | 001, 218, 219, 220, 221, 222, 223, 224, 225, 226, 227, 228, 229 |
| 9(bT) | 001, 218, 219, 220, 221, 222, 223, 224, 225, 226, 227, 228, 229 |
| 9(cT) | 001, 231, 232, 233, 234, 235, 236, 237, 238, 239, 240, 241, 242 |
| 9(dT) | 001, 231, 232, 233, 234, 235, 236, 237, 238, 239, 240, 241, 242 |
| 10(aT) | 001, 155, 156, 157, 159, 161, 163, 165 |
| 10(aB) | 001, 155, 156, 157, 159, 161, 163, 165 |
| 10(bT) | 001, 168, 170, 172, 176, 179, 181 |
| 10(bB) | 001, 168, 170, 172, 176, 179, 181 |
| 11(a) | 001, 82, 86, 87, 88, 90, 91, 92, 94, 95, 96, 105, 106, 107 |
| 11(b) | 001, 82, 86, 87, 88, 90, 91, 92, 94, 95, 96, 105, 106, 107 |
| 11(c) | 001, 115, 116, 117, 118, 119, 120, 122, 123, 124, 125, 126, 127, 128 |
| 11(d) | 001, 115, 116, 117, 118, 119, 120, 122, 123, 124, 125, 126, 127, 128 |
| 12(aT) | 001, 801, 802, 803, 804, 805, 806, 807 |
| 12(aB) | 001, 801, 802, 803, 804, 805, 806, 807 |
| 12(bT) | 001, 792, 793, 794, 795, 796, 797, 798, 799 |
| 12(bB) | 001, 792, 793, 794, 795, 796, 797, 798, 799 |
| 13(a) | 001, 270, 272, 273, 274, 276, 277, 278, 280, 281 |
| 13(b) | 001, 270, 272, 273, 274, 276, 277, 278, 280, 281 |
| 13(c) | 001, 283, 284, 285, 286, 287, 288, 289, 290, 291, 292 |
| 13(d) | 001, 283, 284, 285, 286, 287, 288, 289, 290, 291, 292 |
| | Angle-of-attack variation: |
| 14(aT) | 001, 476, 477, 479, 481 |
| 14(bT) | 001, 446, 449, 450, 451, 452 |
| 14(cT) | 001, 423, 424, 425, 426, 427 |
| 14(dT) | 001, 911, 912, 913, 914, 915 |

^aT indicates top plot on page; B indicates bottom plot on page.

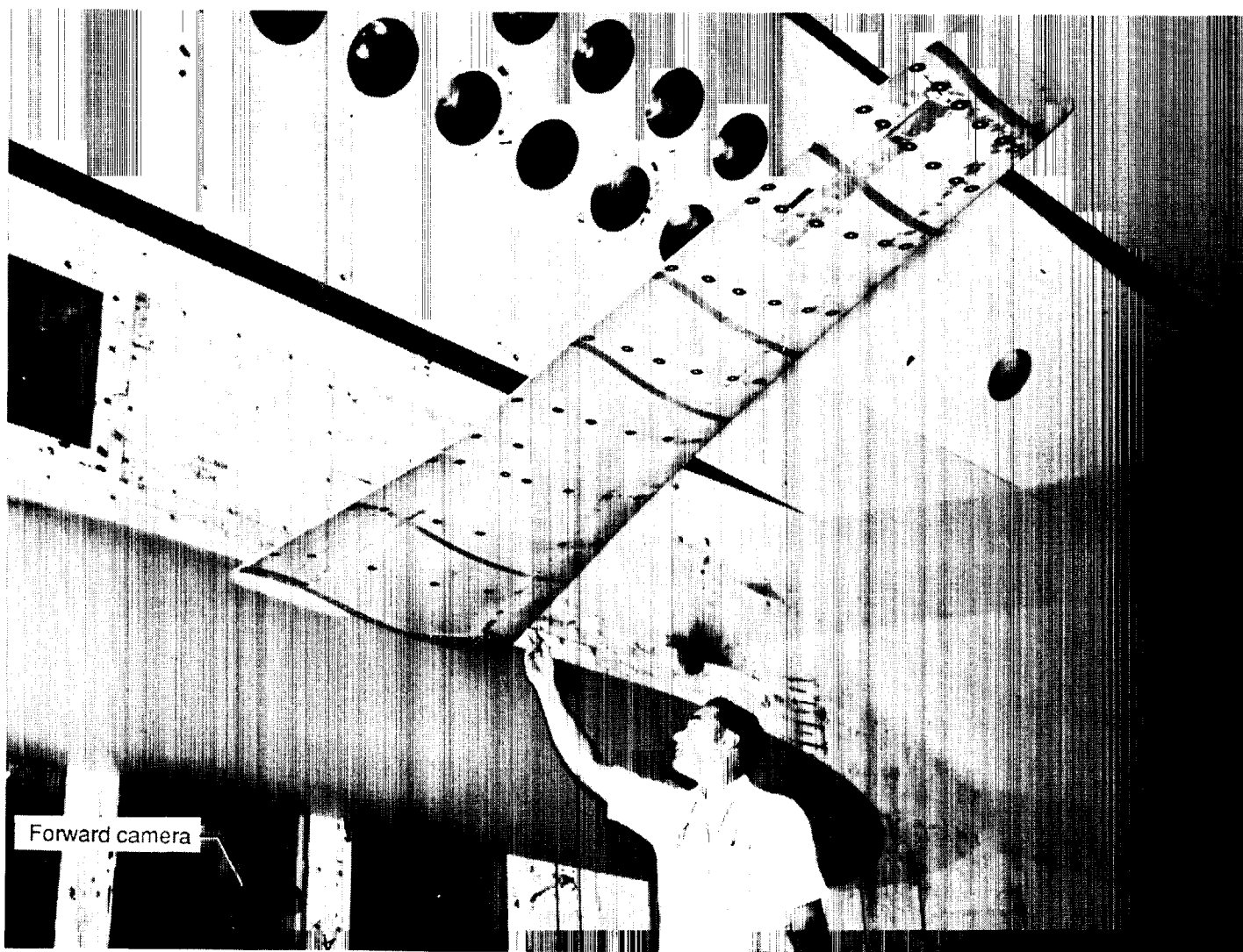
Table 7. Continued

| Figure (a) | Tab point |
|---------------|---|
| | Control surface deflection variation: |
| 15(aT) | 001, 548, 567, 568, 570, 572, 573, 574 |
| 15(aB) | 001, 548, 567, 568, 570, 572, 573, 574 |
| 15(bT) | 001, 482, 483, 484, 485, 486, 487 |
| 15(bB) | 001, 482, 483, 484, 485, 486, 487 |
| 16(a) | 001, 465, 466, 467, 468, 469, 471, 473, 474 |
| 16(b) | 001, 465, 466, 467, 468, 469, 471, 473, 474 |
| 16(c) | 001, 453, 455, 456, 459, 460, 461, 462 |
| 16(d) | 001, 453, 455, 456, 459, 460, 461, 462 |
| 17(a) | 001, 437, 438, 439, 440, 441, 442, 443, 444 |
| 17(b) | 001, 437, 438, 439, 440, 441, 442, 443, 444 |
| 17(c) | 001, 428, 429, 431, 432, 433, 434, 435, 436 |
| 17(d) | 001, 428, 429, 431, 432, 433, 434, 435, 436 |
| 18(a) | 001, 916, 917, 918, 919, 920, 921, 922, 923 |
| 18(b) | 001, 916, 917, 918, 919, 920, 921, 922, 923 |
| 18(c) | 001, 924, 925, 926, 927, 928, 929, 930, 931 |
| 18(d) | 001, 924, 925, 926, 927, 928, 929, 930, 931 |
| | Angle-of-attack variation: |
| 19(a) | 001, 948, 951, 952 |
| 19(b) | 001, 948, 951, 952 |
| | Control surface deflection variation: |
| 20(a) | 001, 953, 955, 957, 958, 959, 960, 961 |
| 20(b) | 001, 953, 955, 957, 958, 959, 960, 961 |
| | Angle-of-attack variation in air: |
| 21(a) | 001, 977, 978, 979, 980, 981, 982, 983 |
| 21(b) | 001, 977, 978, 979, 980, 981, 982, 983 |
| | Control surface deflection variation in air: |
| 22(a) | 001, 1004, 1005, 1006, 1007, 1008, 1009, 1010, 1011 |
| 22(b) | 001, 1004, 1005, 1006, 1007, 1008, 1009, 1010, 1011 |
| 22(c) | 001, 1012, 1013, 1014, 1015, 1016, 1018, 1019, 1020 |
| 22(d) | 001, 1012, 1013, 1014, 1015, 1016, 1018, 1019, 1020 |

^aT indicates top plot on page; B indicates bottom plot on page.

Table 7. Concluded

| Figure | Tab point |
|--------|--|
| | Angle-of-attack variation: |
| 23(a) | 211, 212, 213, 214, 215, 216 |
| 23(b) | 148, 149, 150, 151, 152, 153, 154 |
| 23(c) | 80, 81, 82, 108, 109, 110, 111 |
| 23(d) | 783, 784, 785, 788, 789, 790, 791 |
| 24(a) | 476, 477, 479, 481 |
| 24(b) | 446, 449, 450, 451, 452 |
| 24(c) | 423, 424, 425, 426, 427 |
| 24(d) | 911, 912, 913, 914, 915 |
| 25 | 948, 951, 952 |
| | Control surface deflection variation: |
| 26(a) | 217, 218, 219, 220, 221, 222, 223, 224, 225, 226, 227, 228, 229 230, 231, 232, 233, 234, 235, 236, 237, 238, 239, 240, 241, 242 |
| 26(b) | 168, 170, 172, 176, 179, 181, 155, 156, 157, 159, 161, 163, 165 |
| 26(c) | 82, 86, 87, 88, 90, 91, 92, 94, 95, 96, 105, 106, 107 115, 116, 117, 118, 119, 120, 122, 123, 124, 125, 126, 127, 128 |
| 26(d) | 792, 793, 794, 795, 796, 797, 798, 801, 802, 803, 804, 805, 806, 807 |
| 26(e) | 268, 270, 272, 273, 274, 276, 277, 278, 280, 281 283, 284, 285, 286, 287, 288, 289, 290, 291, 292, 293 |
| 27(a) | 548, 566, 567, 568, 570, 572, 573, 574, 482, 483, 484, 485, 486, 487 |
| 27(b) | 465, 466, 467, 468, 469, 471, 473, 474, 453, 455, 456, 459, 460, 461, 462 |
| 27(c) | 428, 429, 431, 432, 433, 434, 435, 436, 437, 438, 439, 440, 441, 442, 443, 444 |
| 27(d) | 916, 917, 918, 919, 920, 921, 922, 923, 924, 925, 926, 927, 928, 929, 930, 931, 932 |
| 28 | 953, 955, 957, 958, 959, 960, 961 |

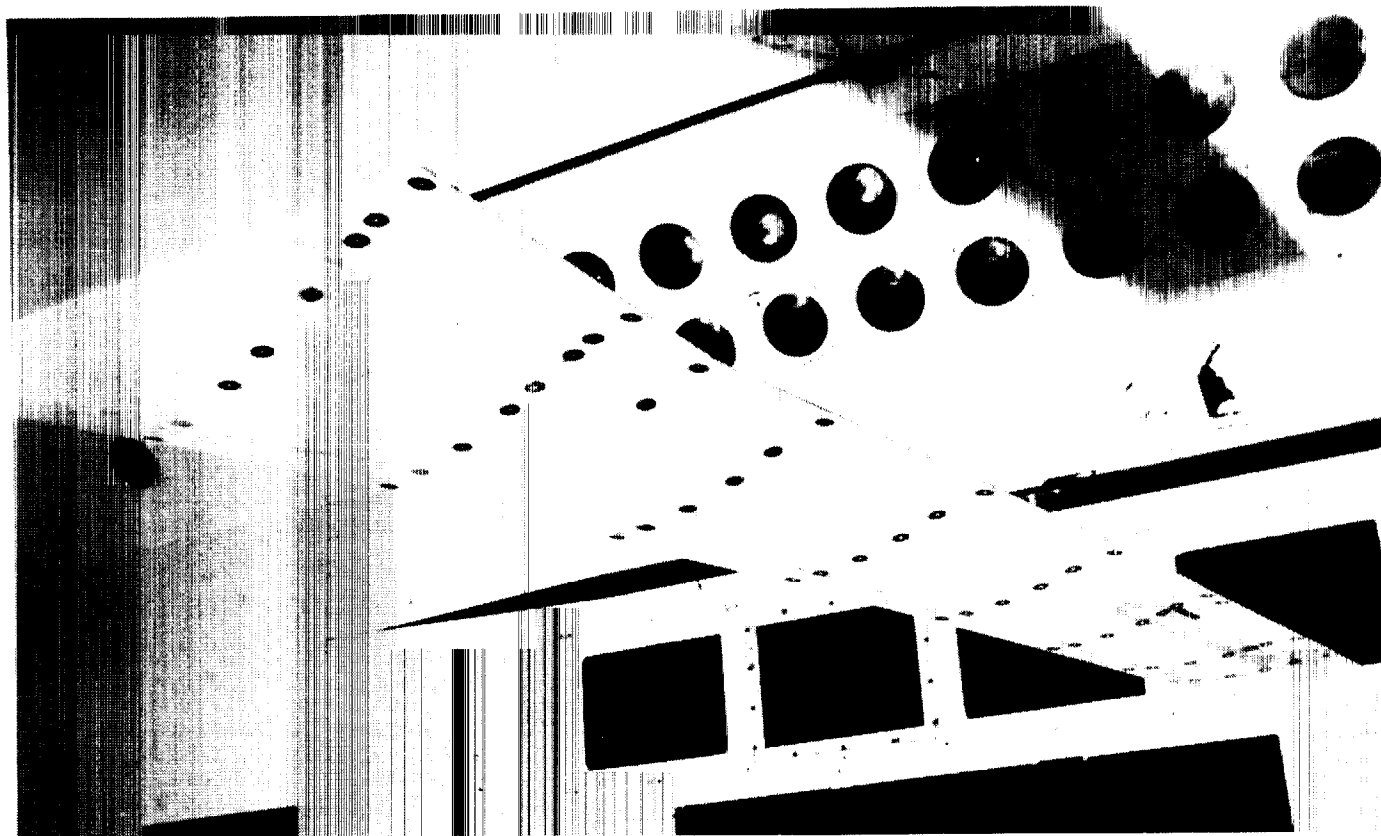


L-90-44

(a) Wing-fuselage assembly in test section.

Figure 1. Test configuration in Langley Transonic Dynamics Tunnel.

ORIGINAL PAGE
BLACK AND WHITE PHOTOGRAPH



L-90-45

(b) Aft-camera view of test wing.

Figure 1. Concluded.

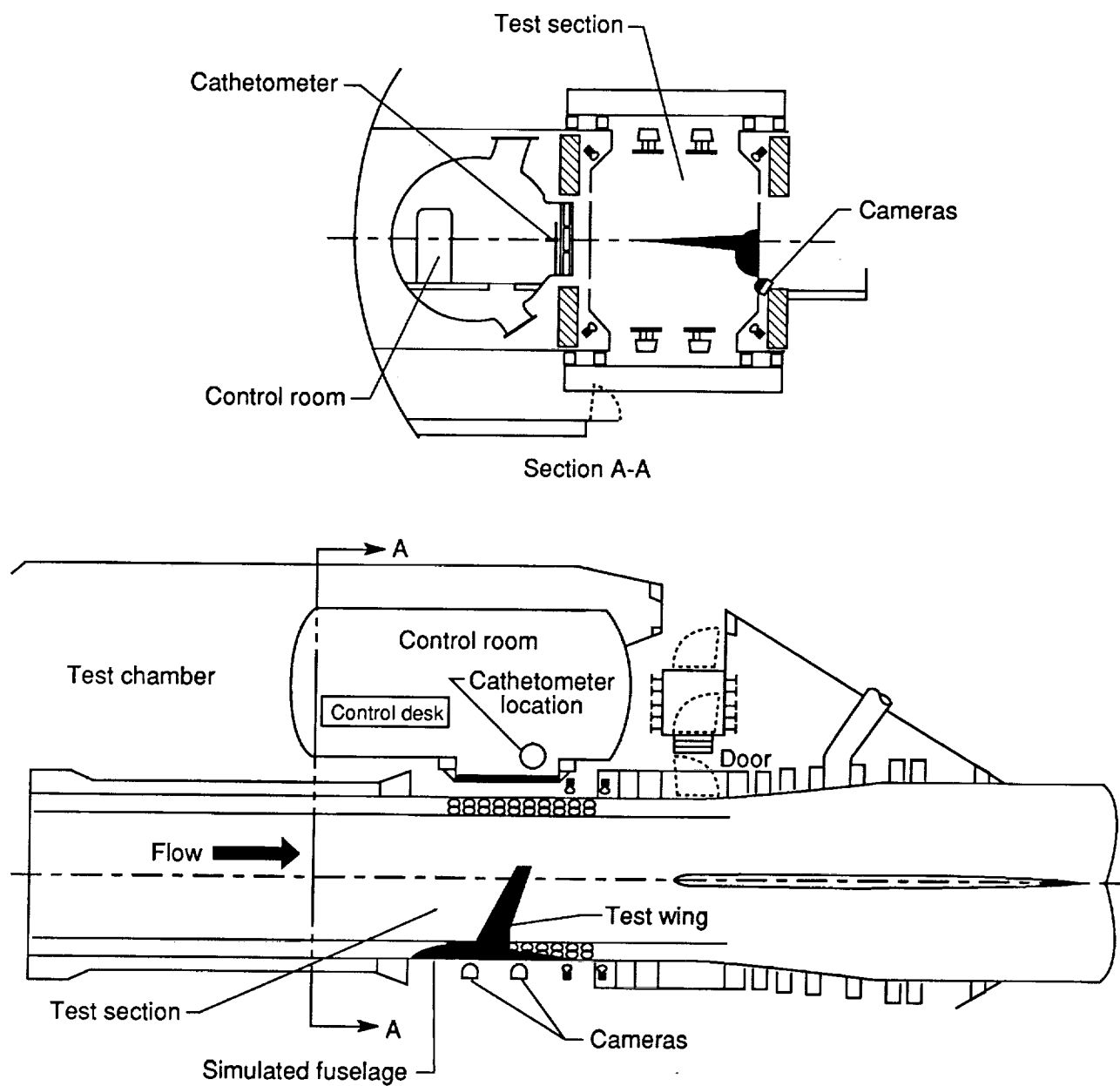


Figure 2. Plan view of wing-fuselage assembly, test section, and control room in test chamber of Langley Transonic Dynamics Tunnel.

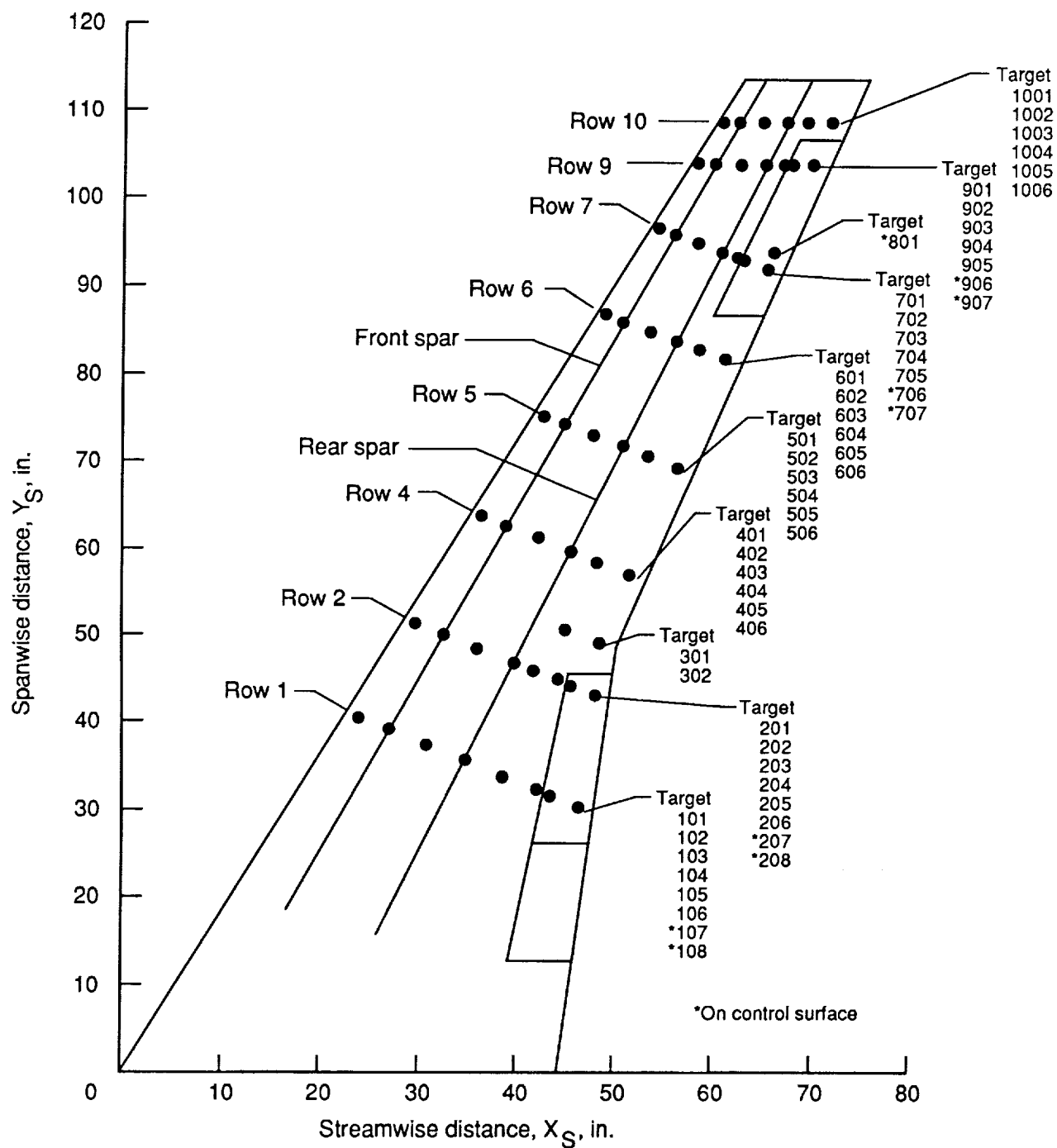


Figure 3. Wing planform showing relative location of targets on wing lower surface. Targets are numbered from leading edge to trailing edge.

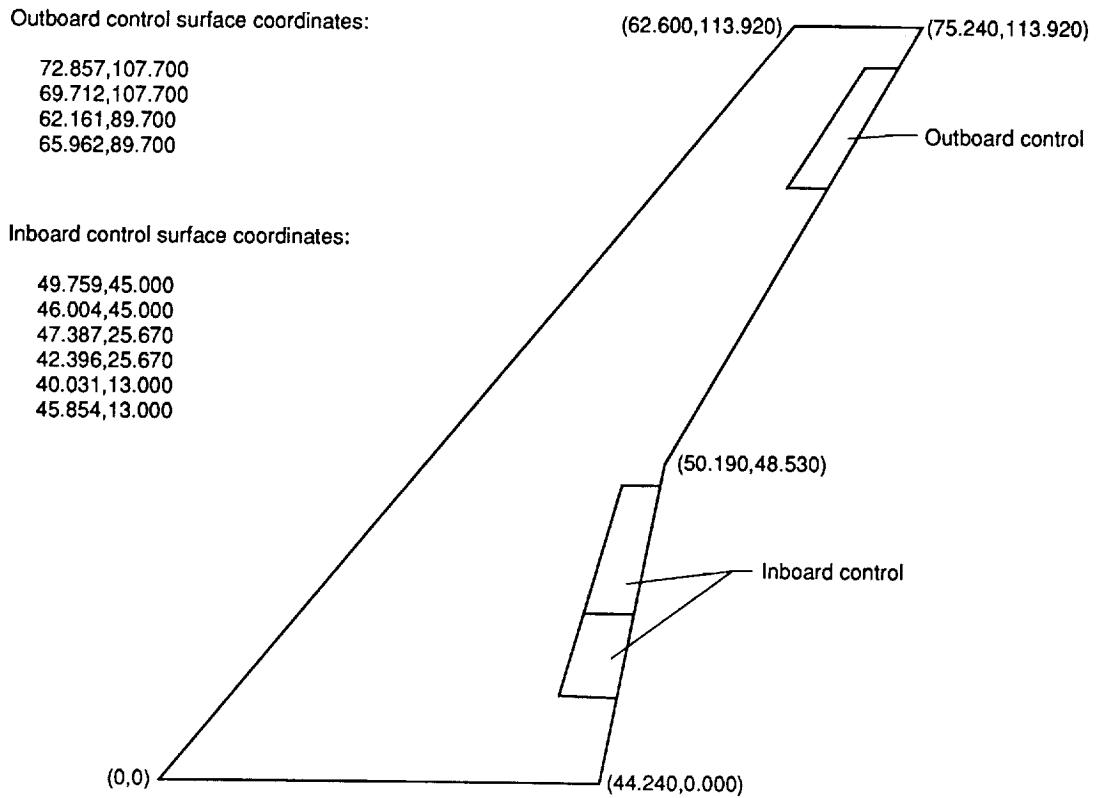


Figure 4. Wing planform and control surfaces locations.

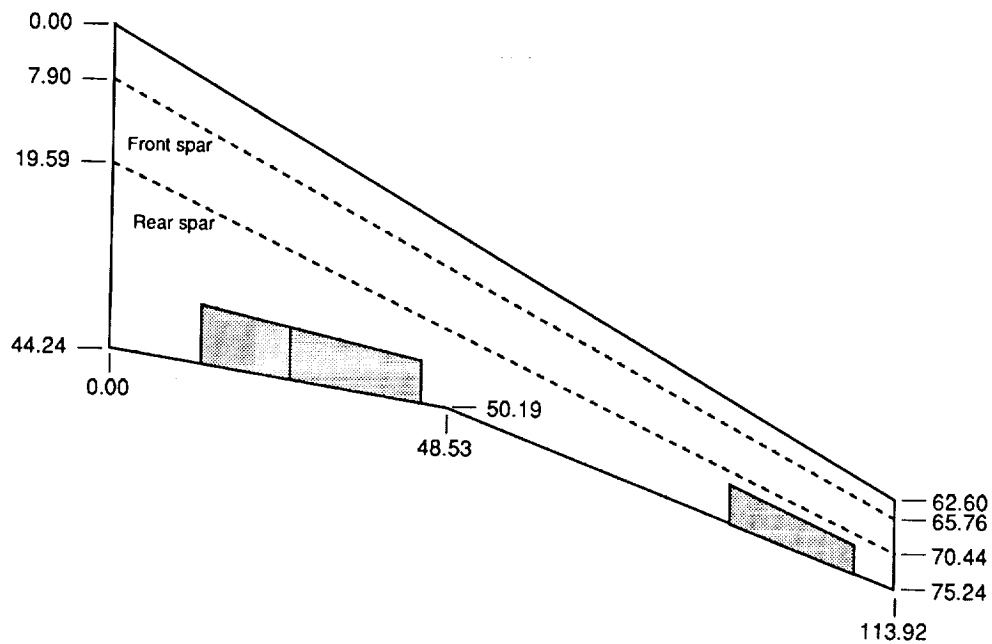


Figure 5. Front and rear spar centerline locations on wing planform. Dimensions are in inches.

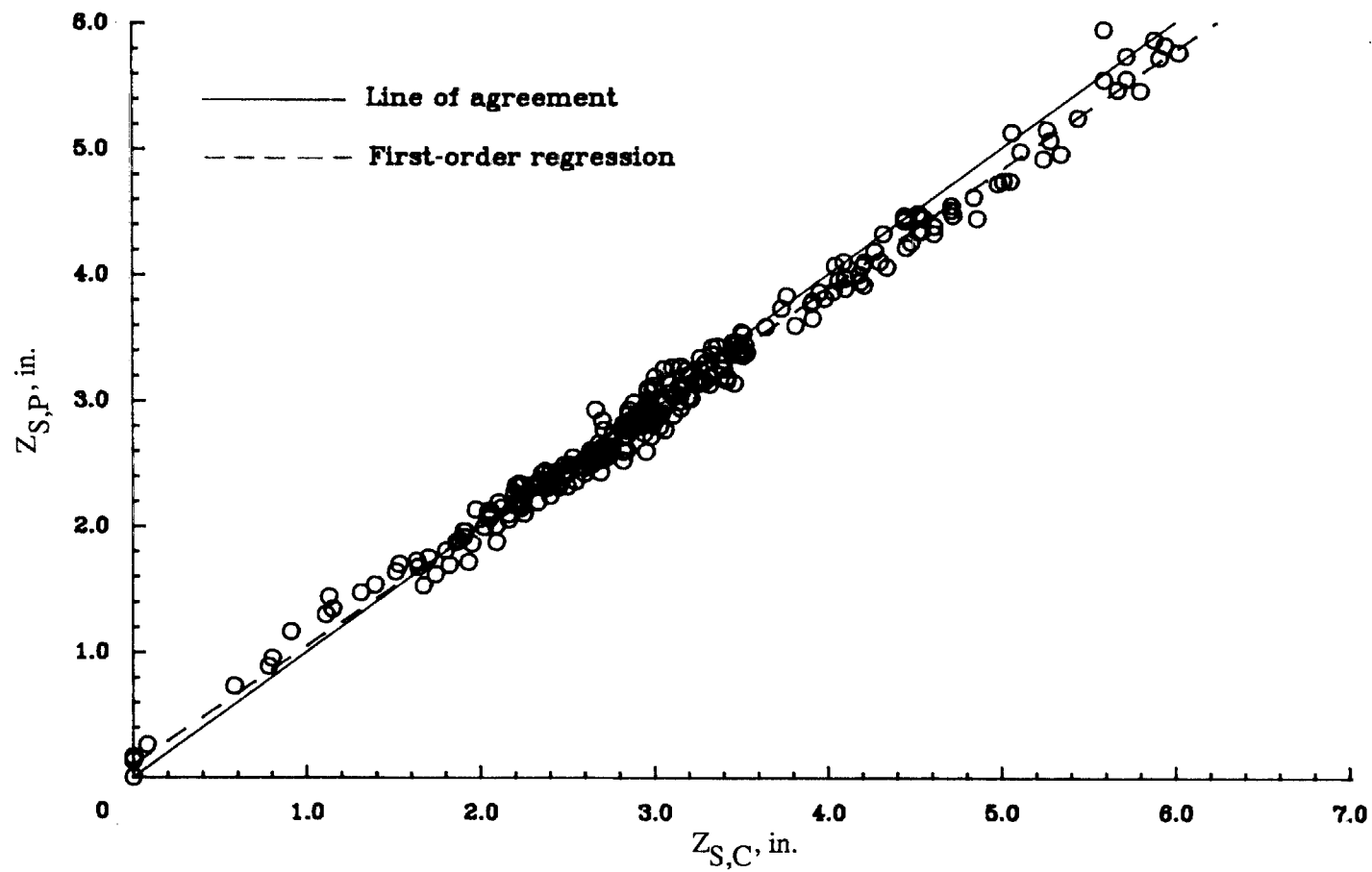
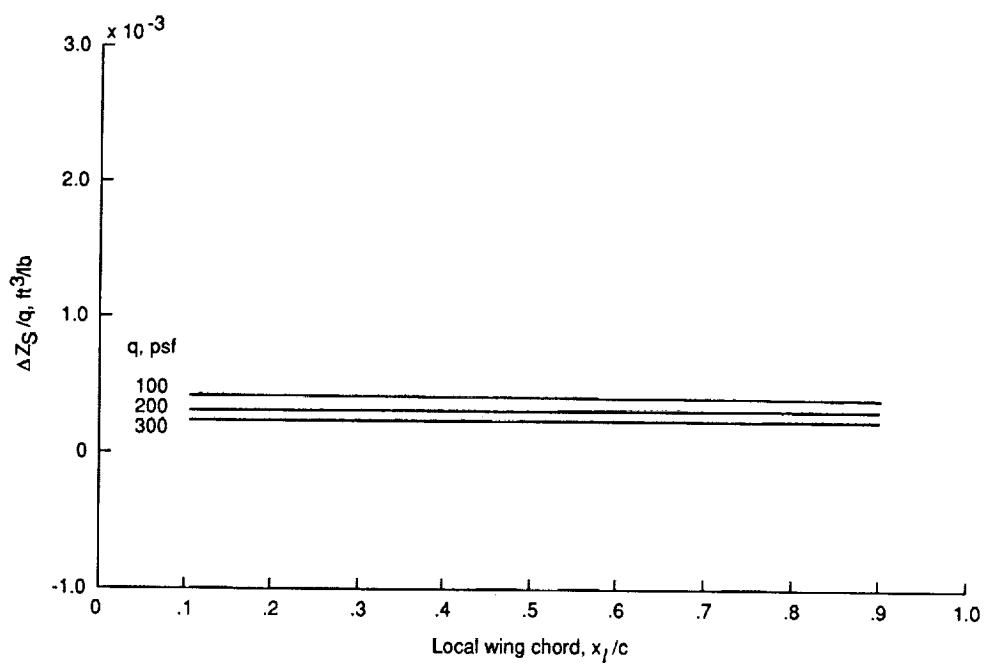
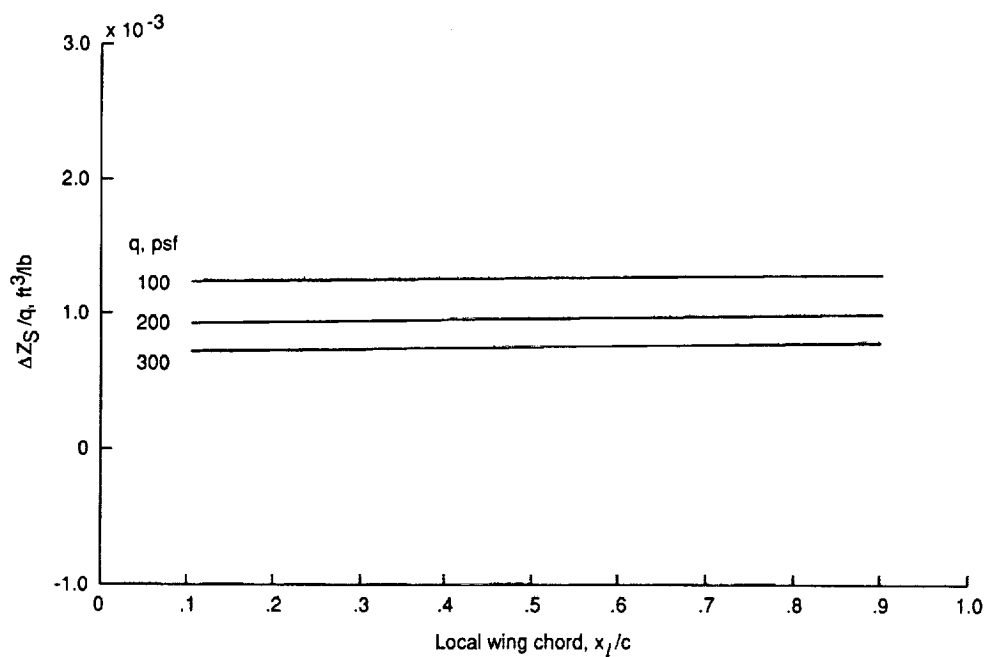


Figure 6. Photogrammetric and cathetometric results for wingtip measurements. $a_0 = 0.10260$; $a_1 = 0.94540$; $C_{cor} = 0.99445$.

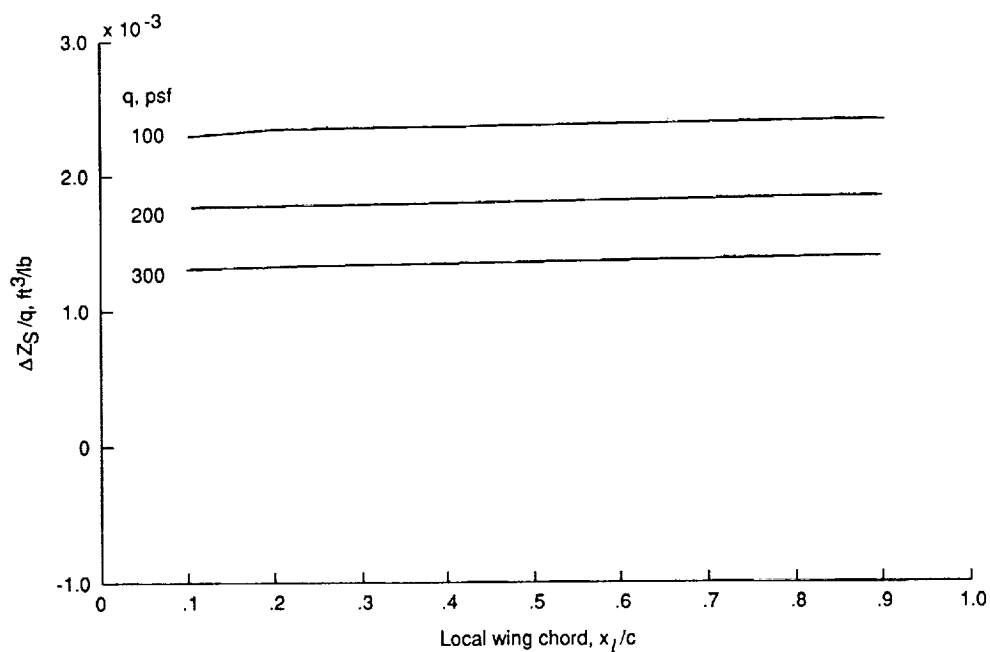


(a) Target row 2.

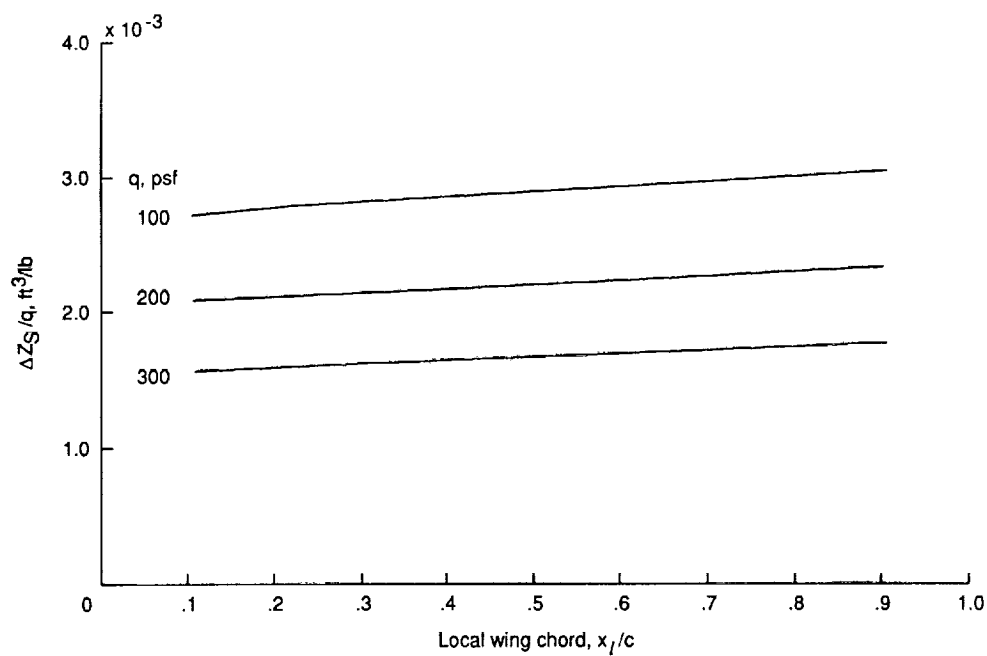


(b) Target row 5.

Figure 7. Effect of dynamic pressure on wing chordwise deflection at selected rows of targets along span at $M = 0.850$ and $\alpha = 1^\circ$.

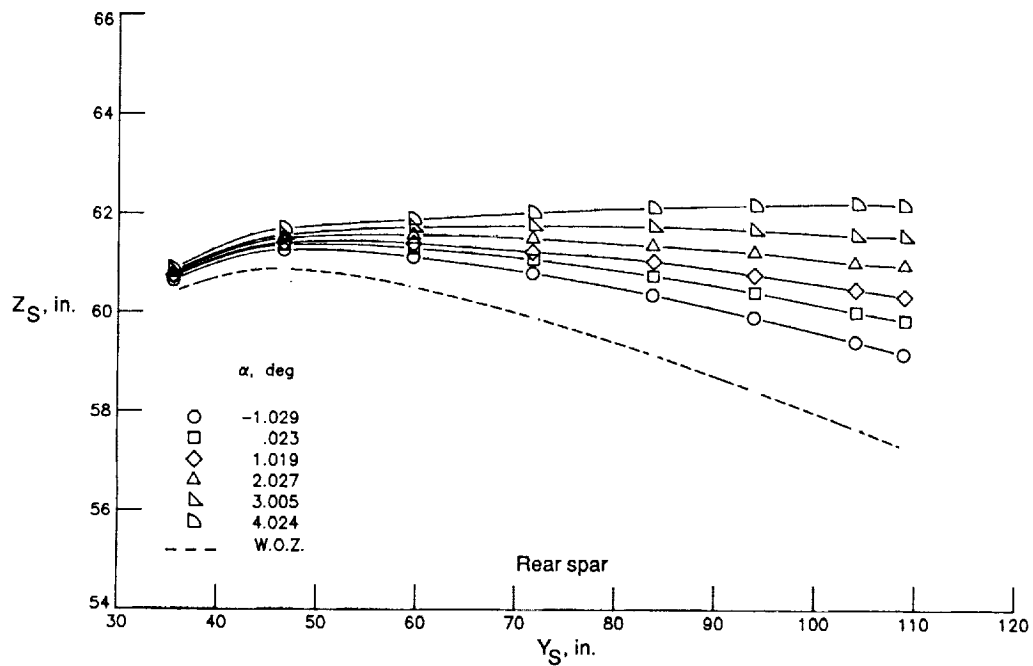
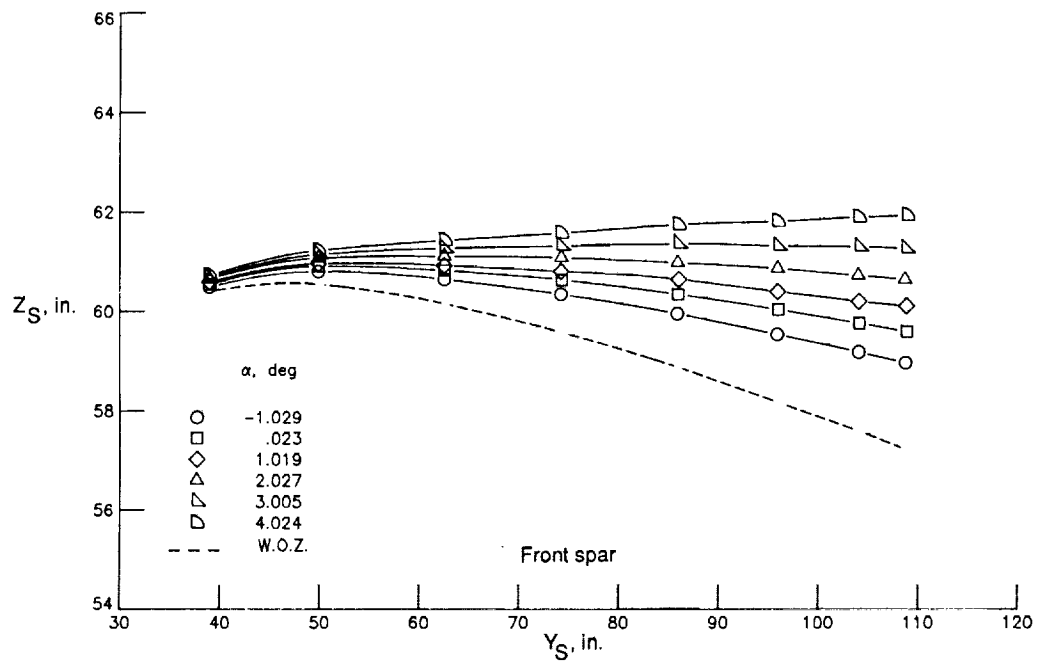


(c) Target row 7.



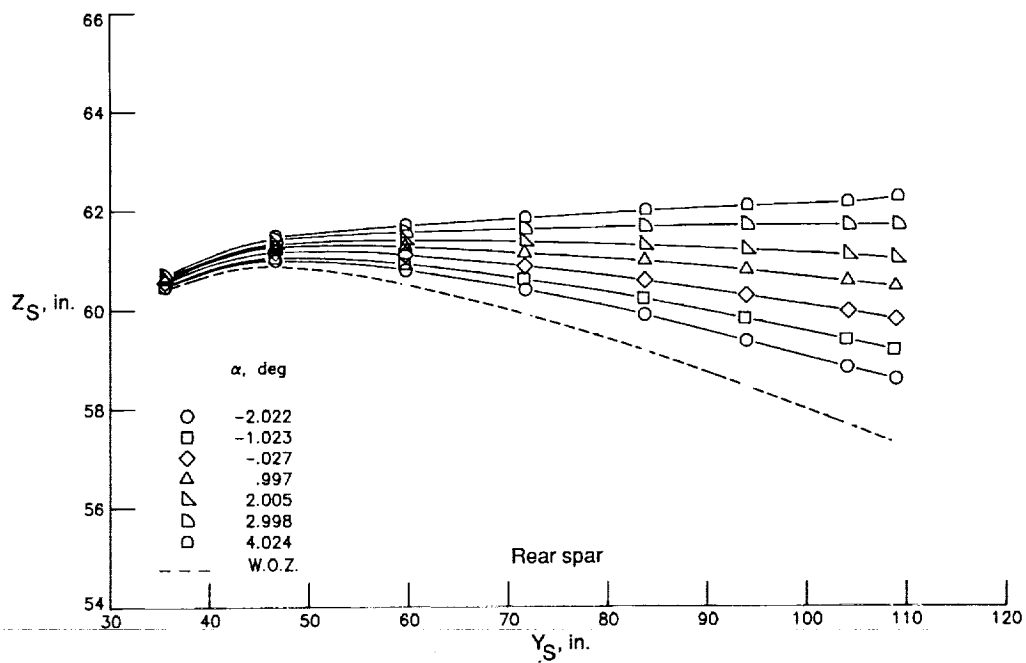
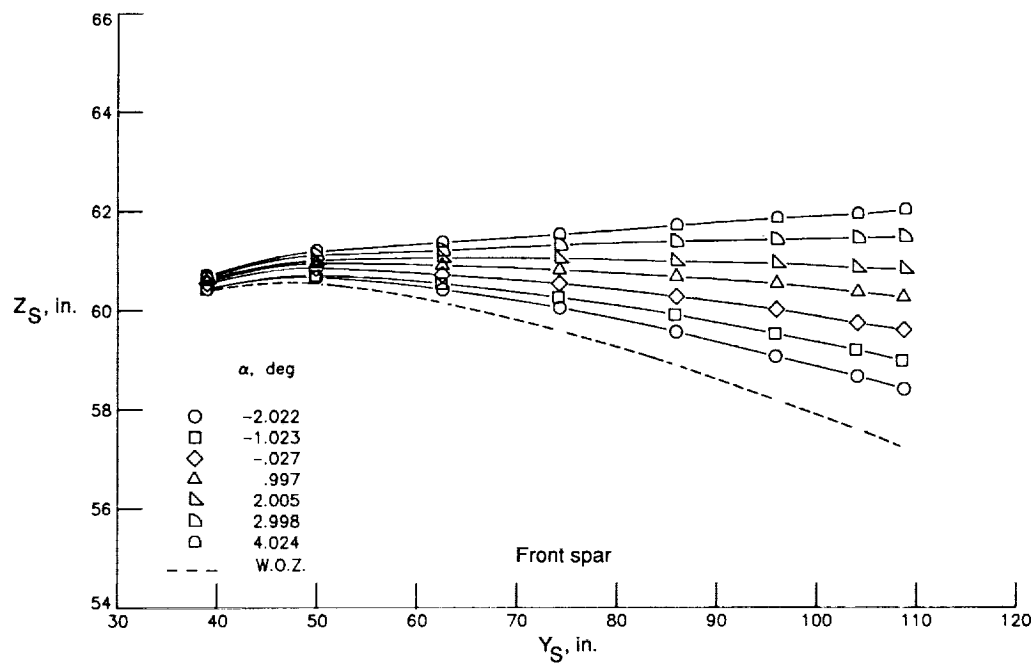
(d) Target row 9.

Figure 7. Concluded.



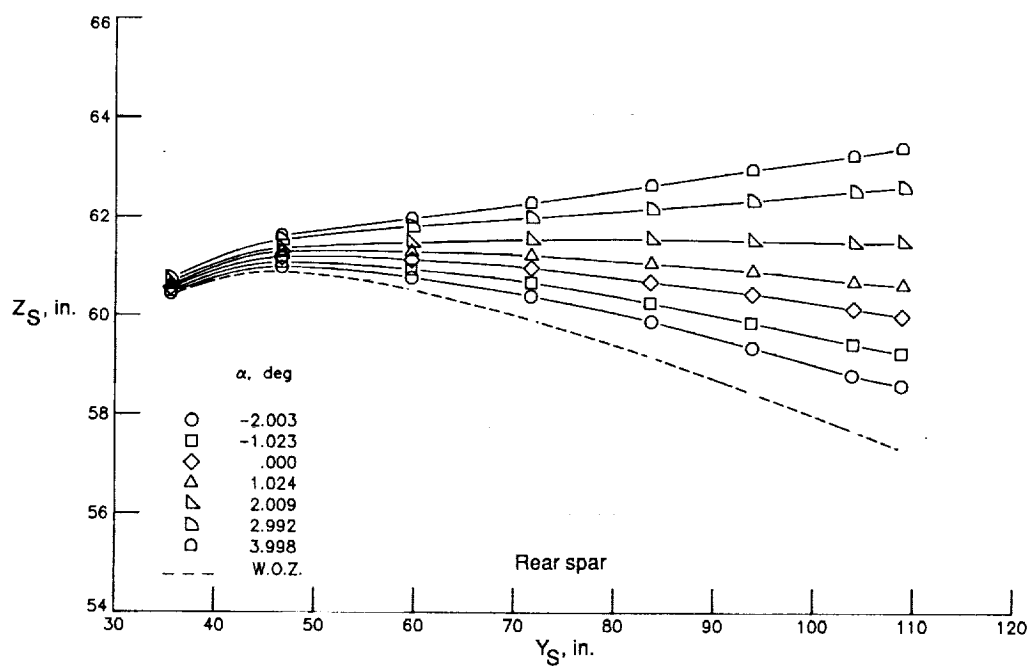
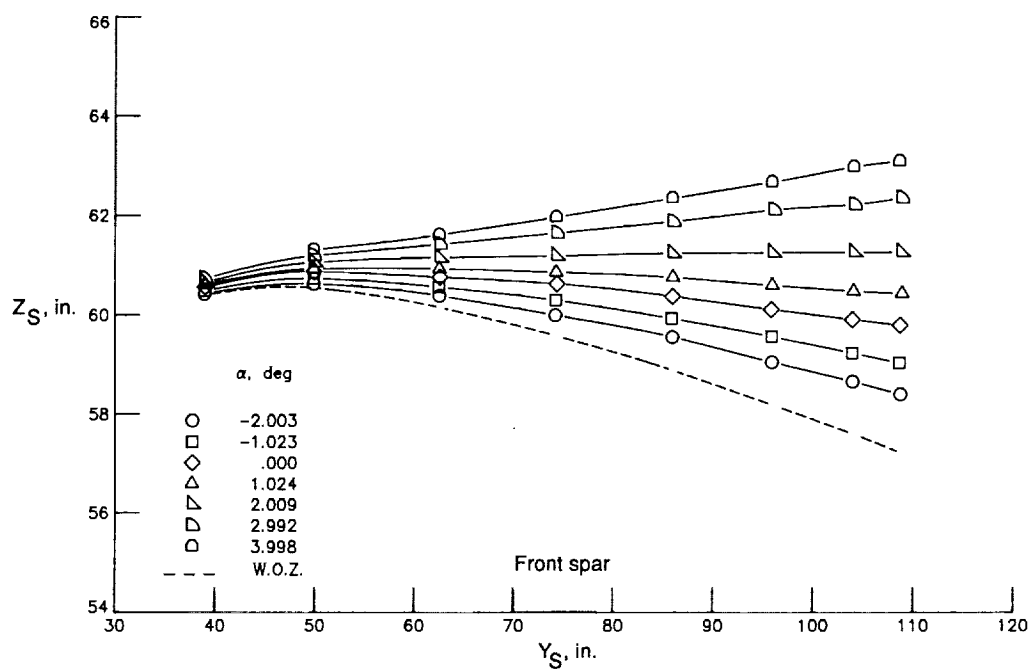
(a) $M = 0.600$.

Figure 8. Variation of wing front and rear spar shapes with angle of attack at four Mach numbers and $q = 100$ psf.



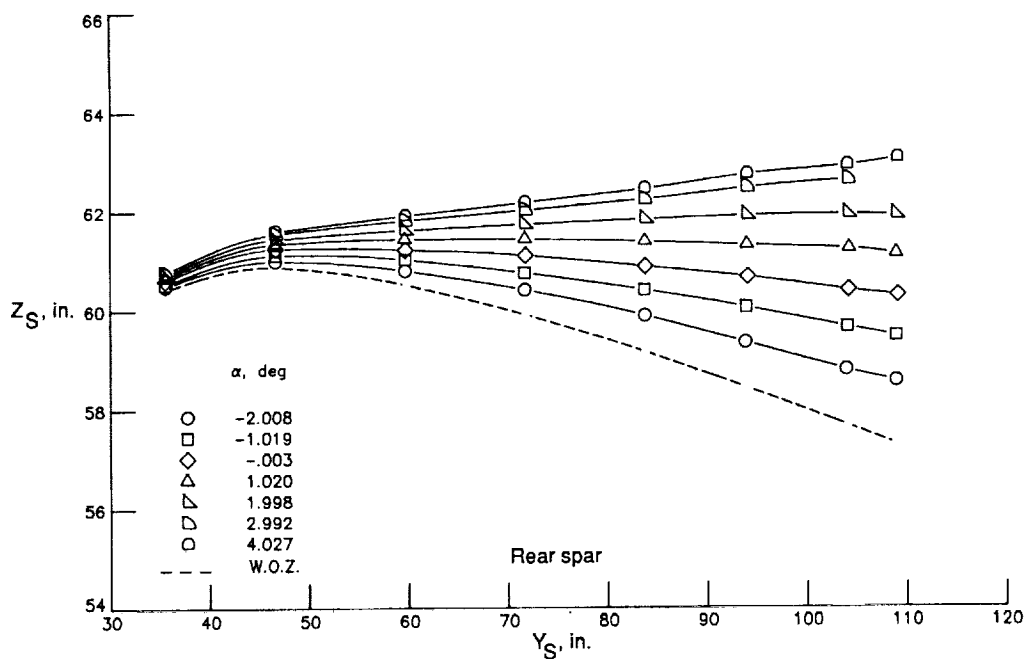
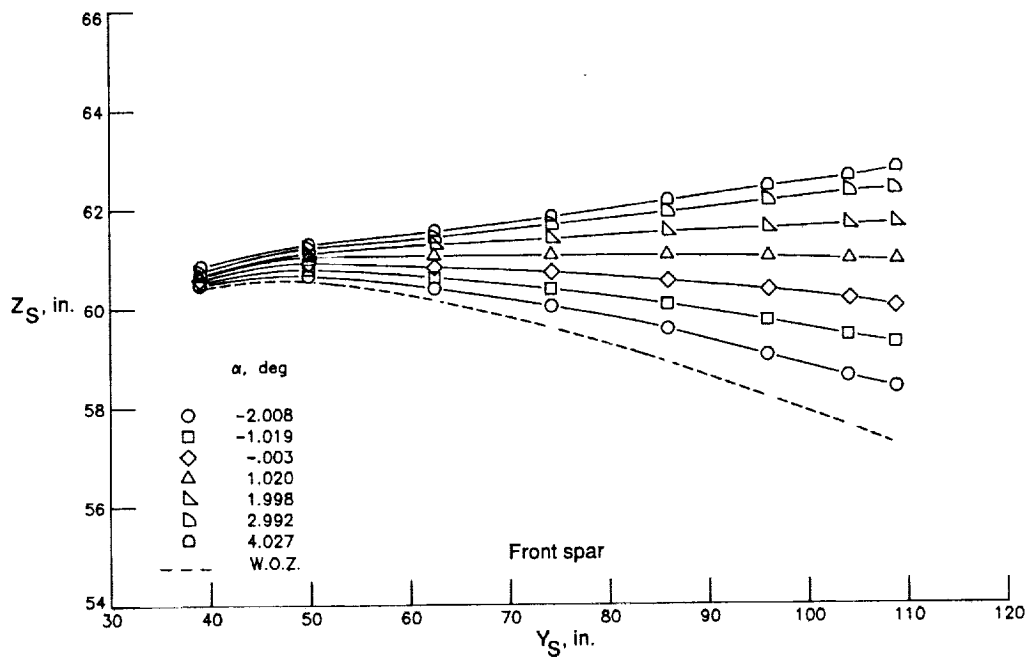
(b) $M = 0.700$.

Figure 8. Continued.



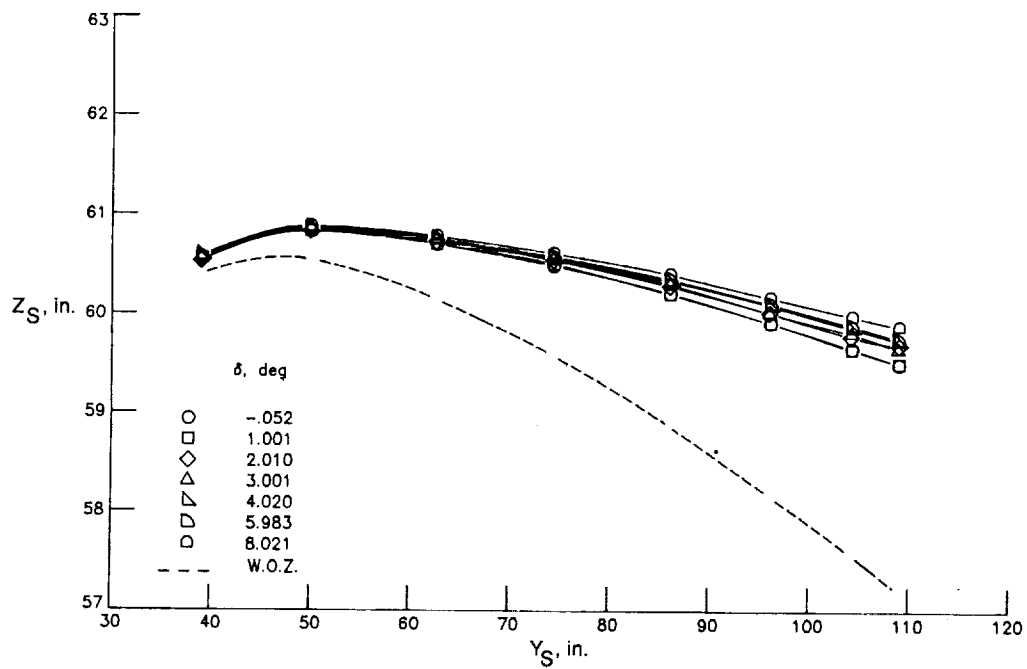
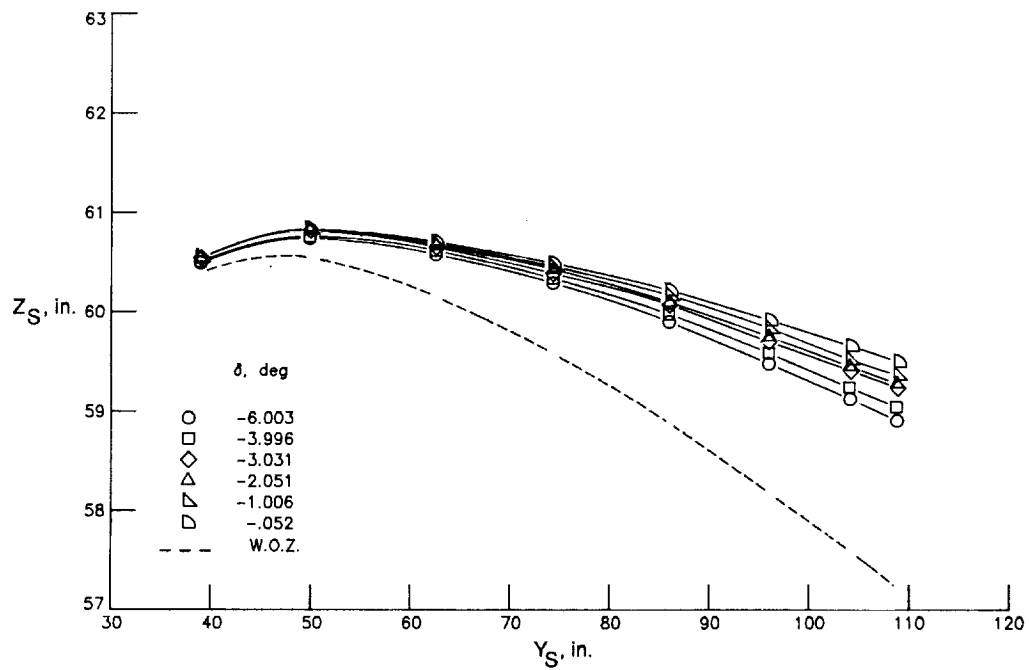
(c) $M = 0.800$.

Figure 8. Continued.



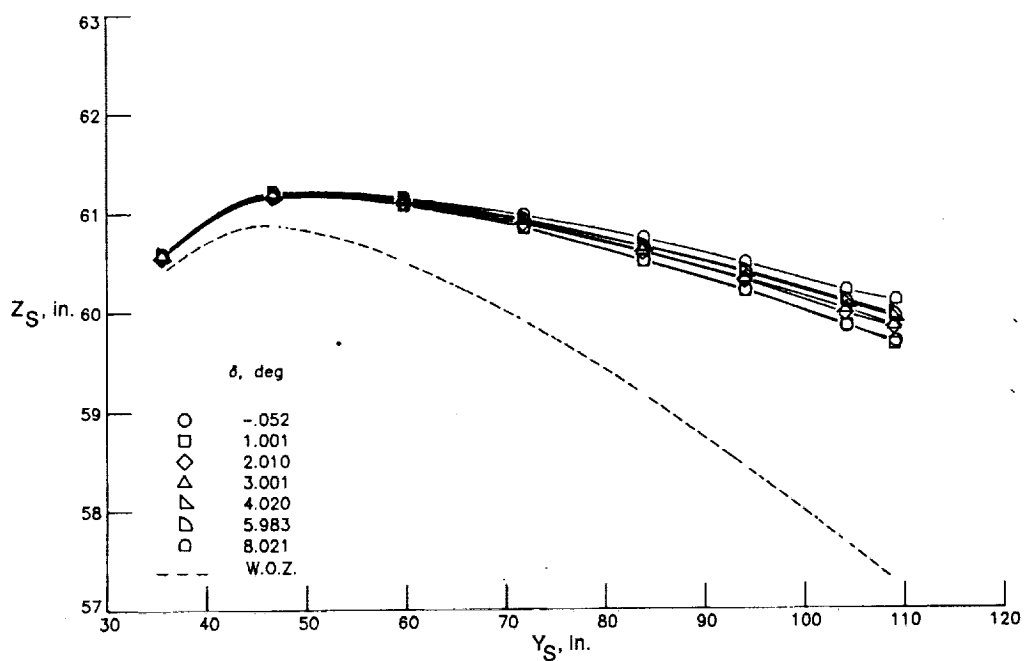
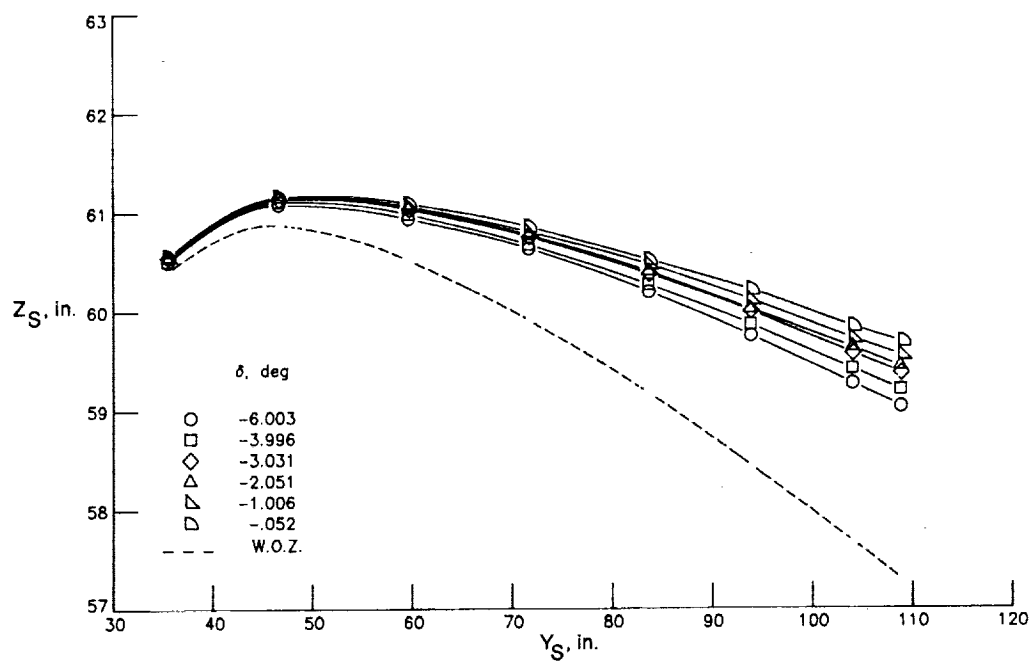
(d) $M = 0.850$.

Figure 8. Concluded.



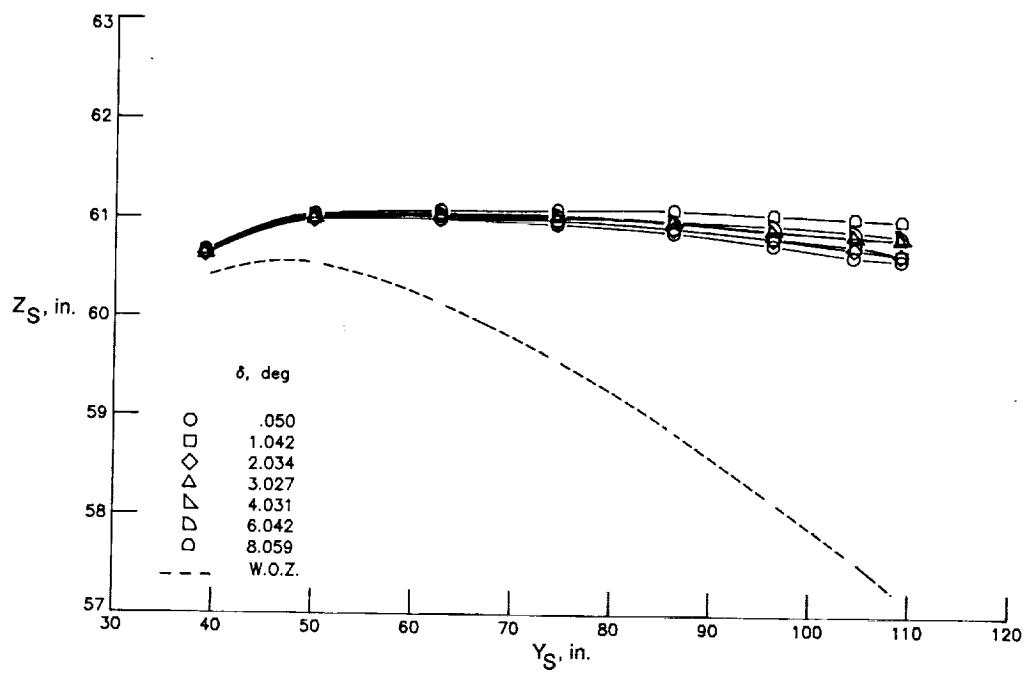
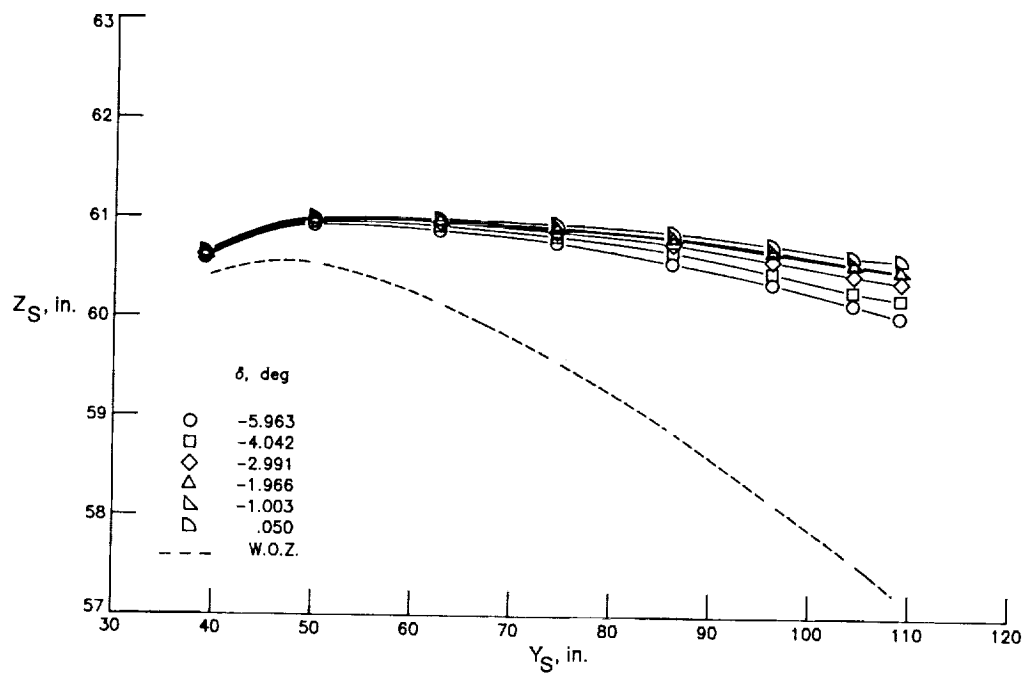
(a) Front spar; $\alpha = 0^\circ$.

Figure 9. Variation of wing front and rear spar shapes with control surface deflection at two angles of attack, $q = 100$ psf, and $M = 0.600$.



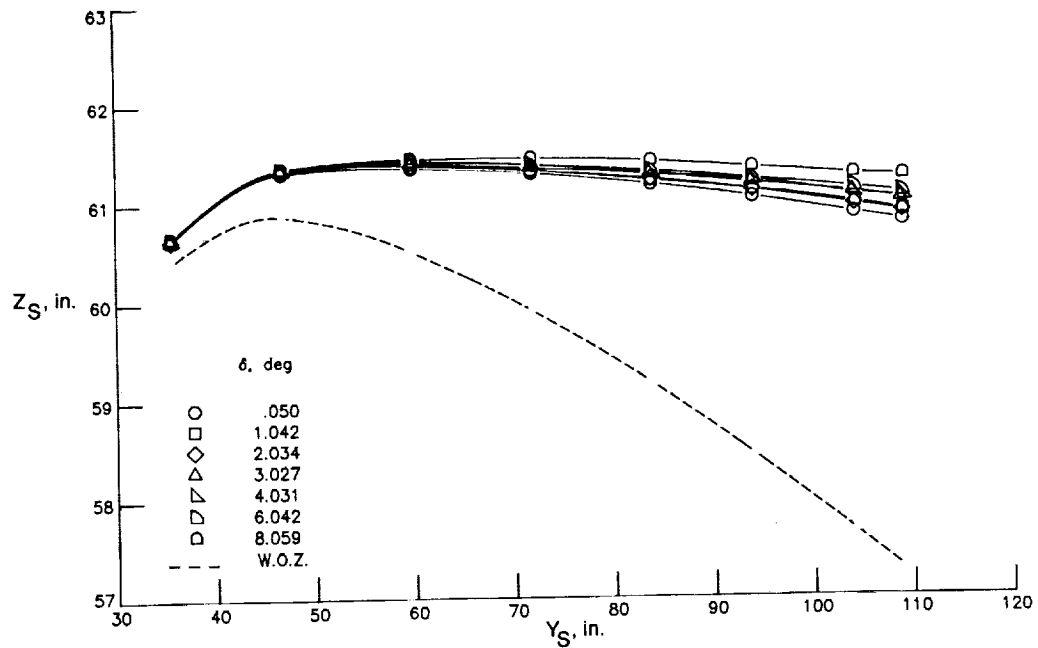
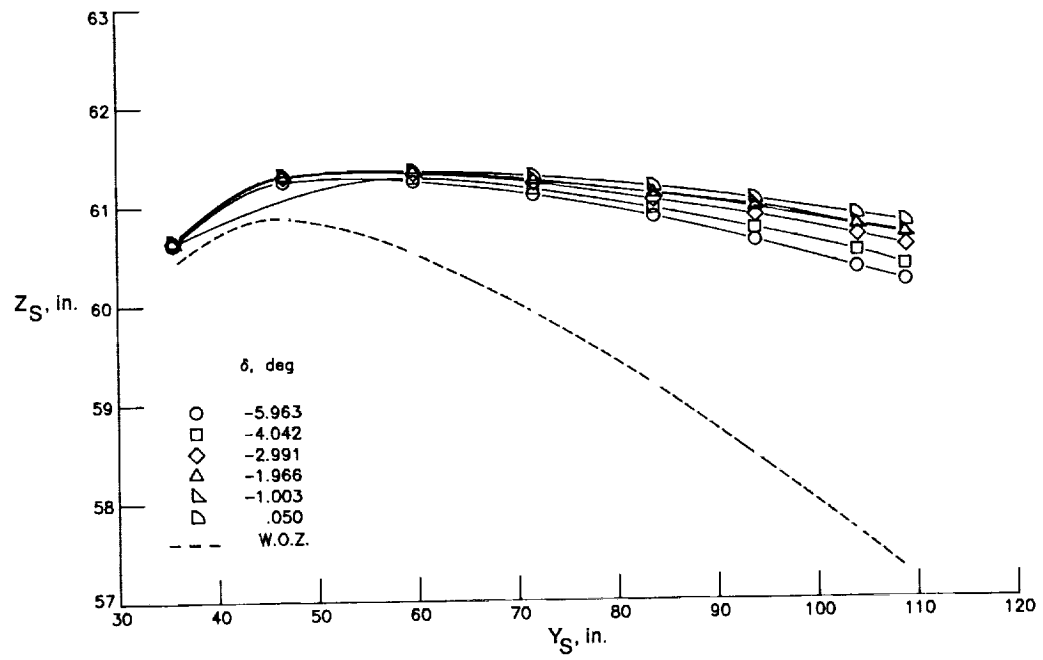
(b) Rear spar; $\alpha = 0^\circ$.

Figure 9. Continued.



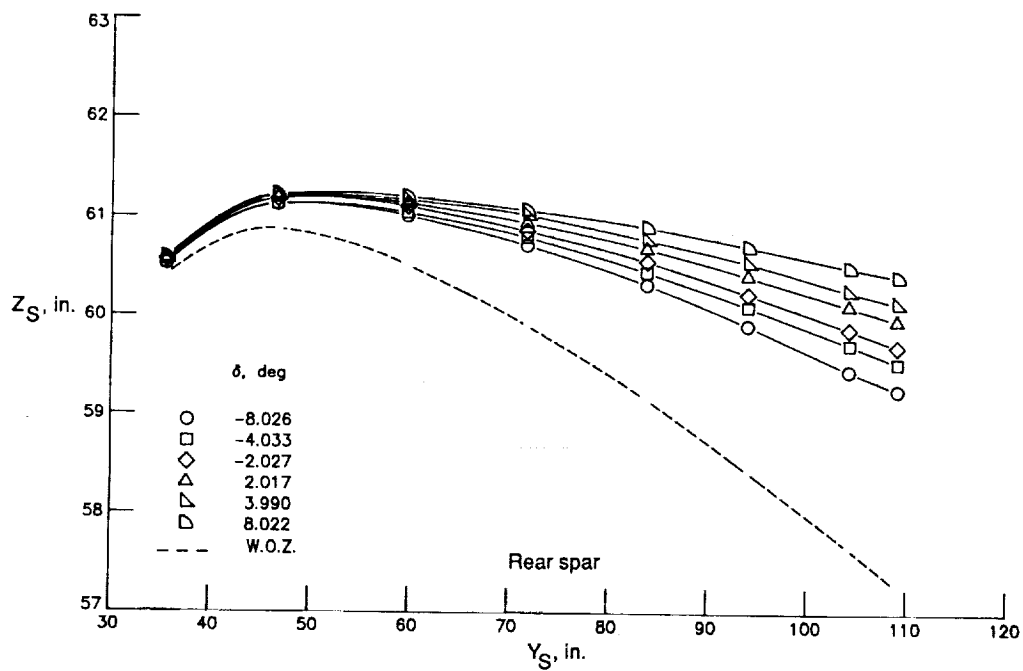
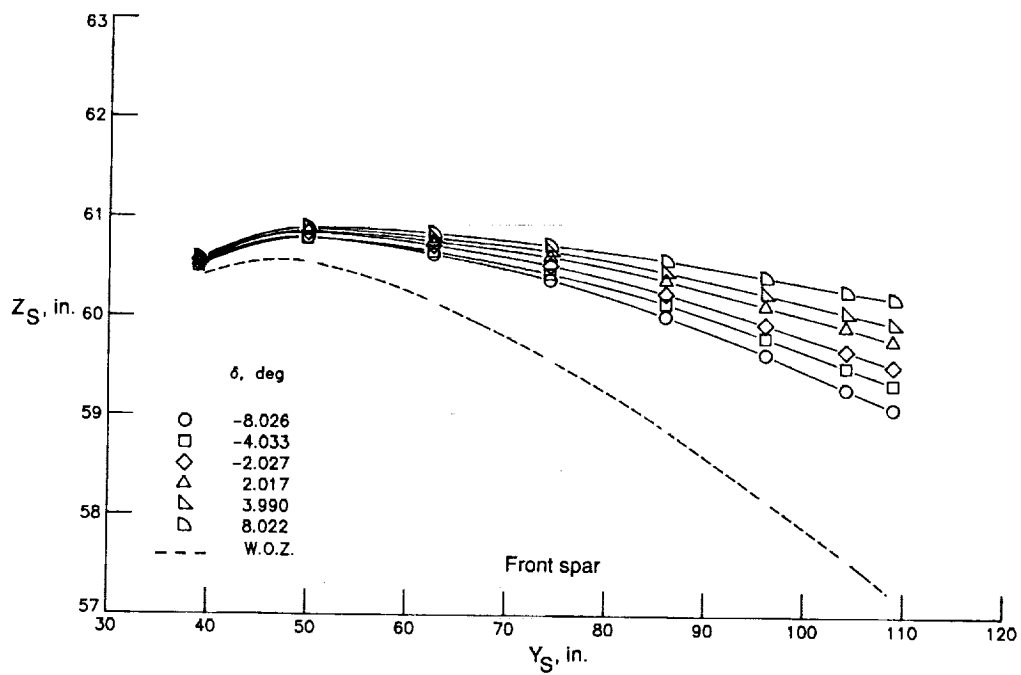
(c) Front spar; $\alpha = 2^\circ$.

Figure 9. Continued.



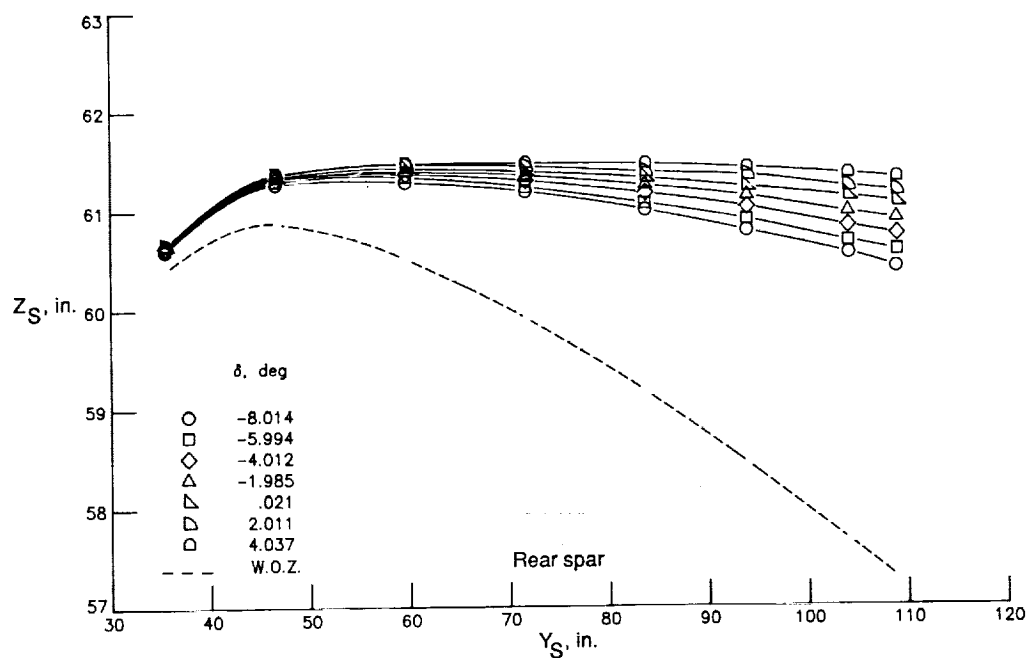
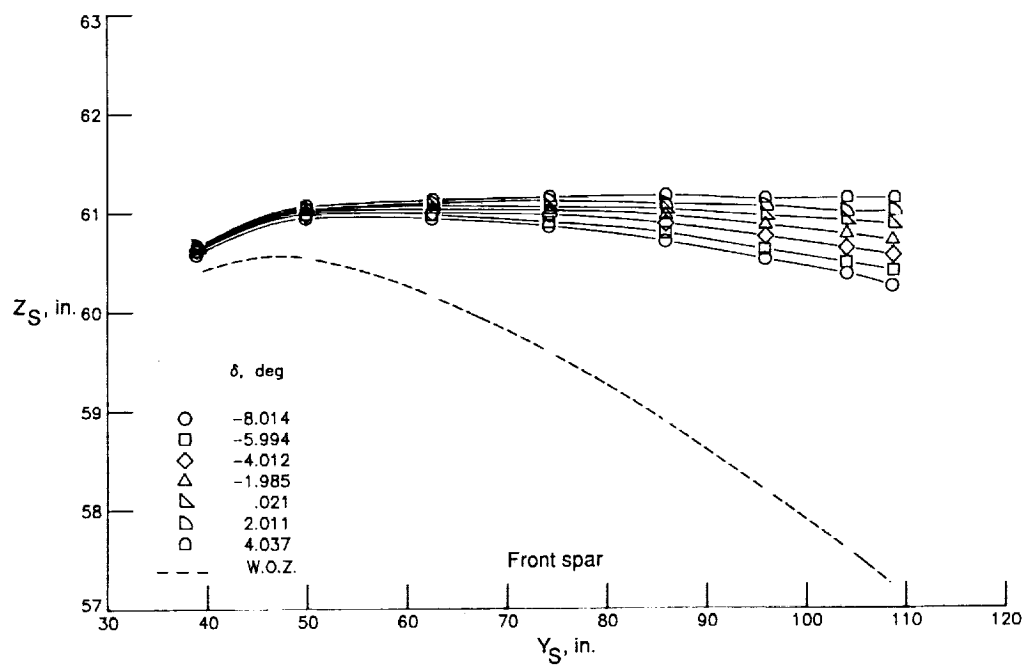
(d) Rear spar; $\alpha = 2^\circ$.

Figure 9. Concluded.



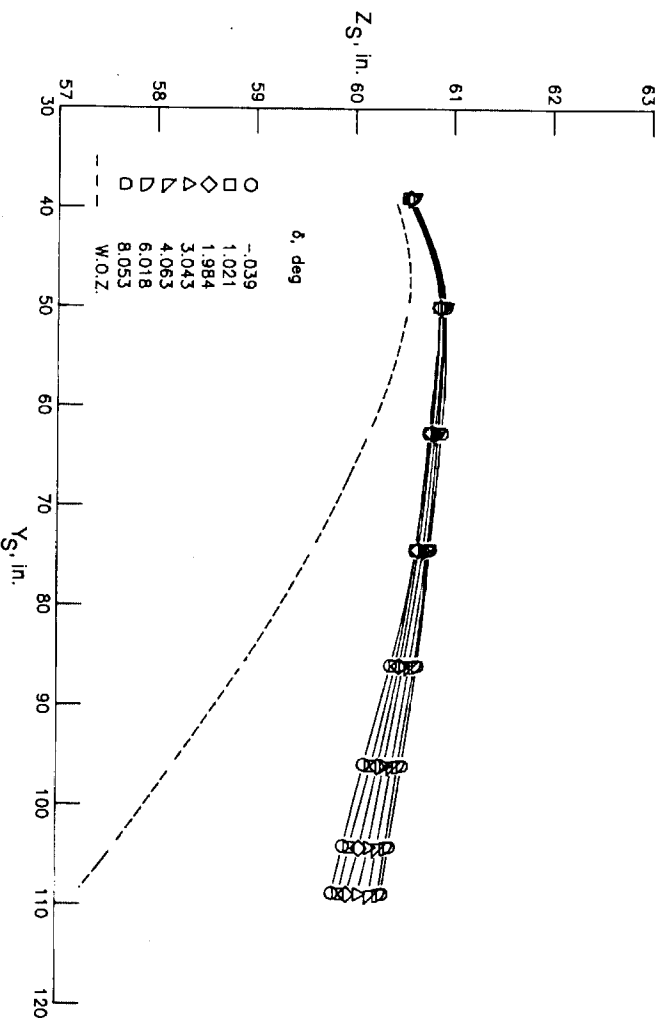
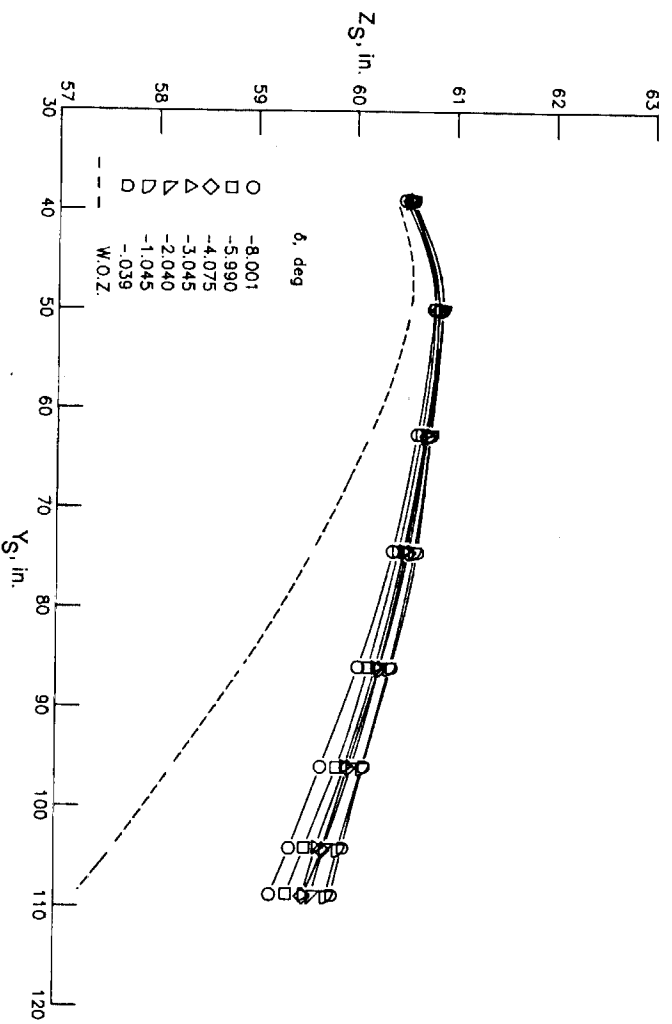
(a) $\alpha = 0^\circ$.

Figure 10. Variation of wing front and rear spar shapes with control surface deflection at two angles of attack, $q = 100$ psf, and $M = 0.700$.



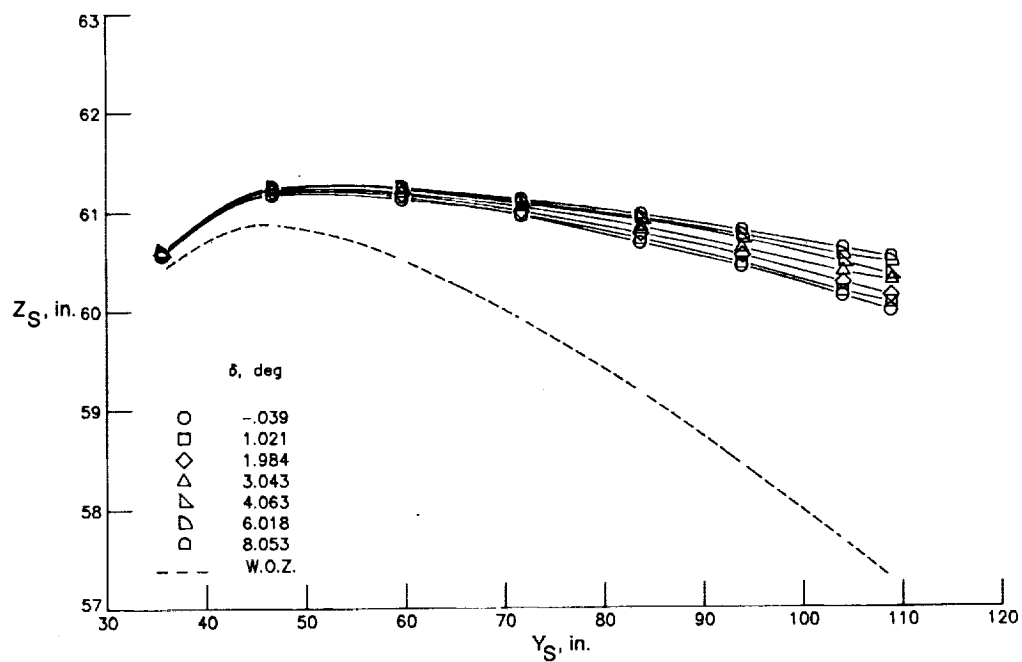
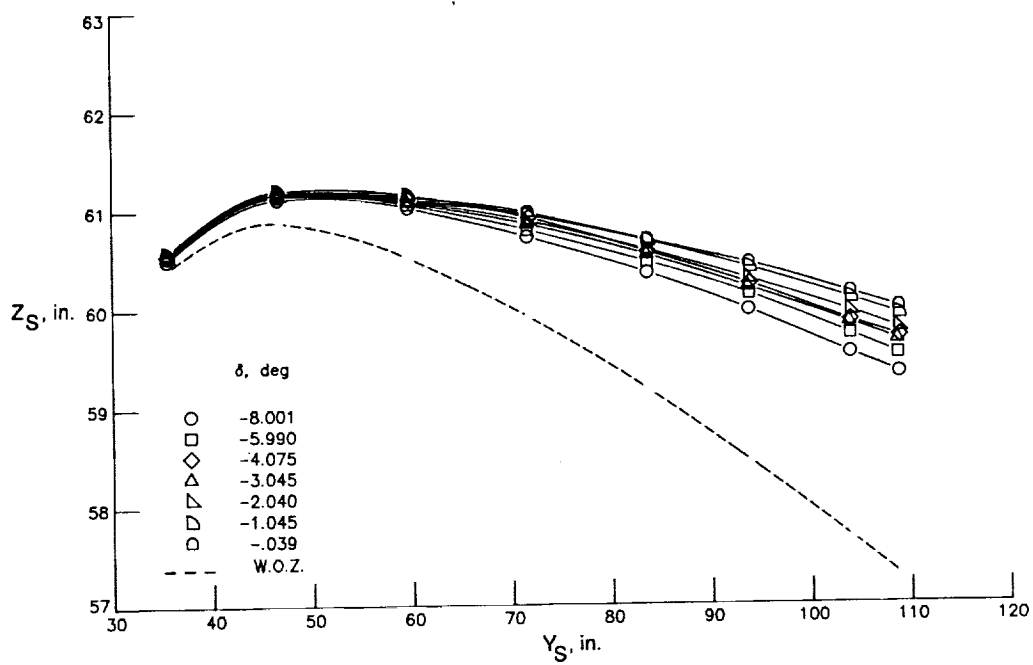
(b) $\alpha = 2^\circ$.

Figure 10. Concluded.



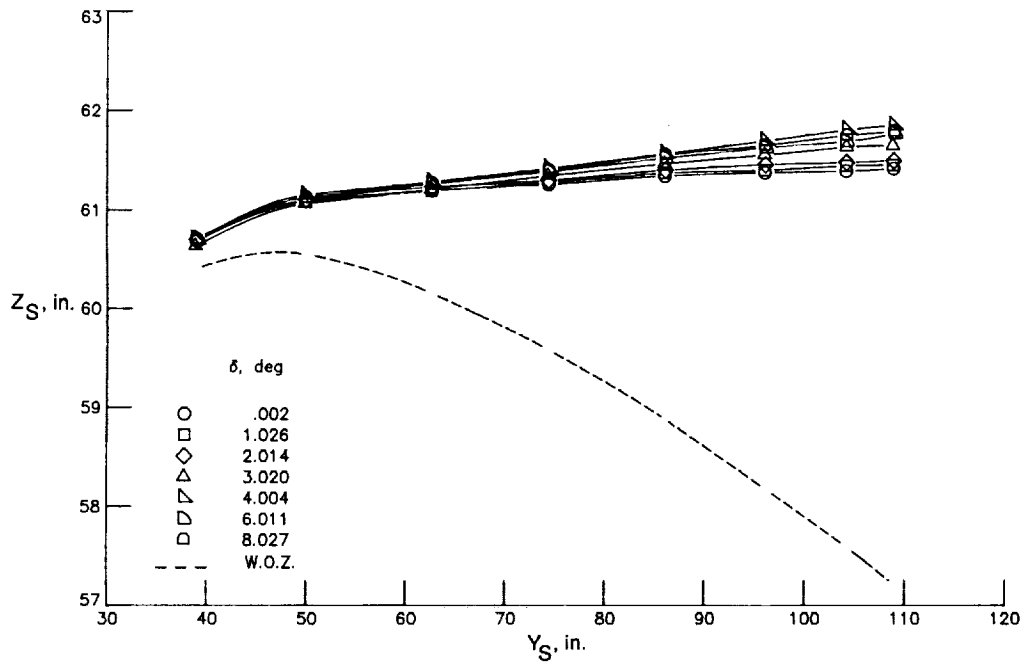
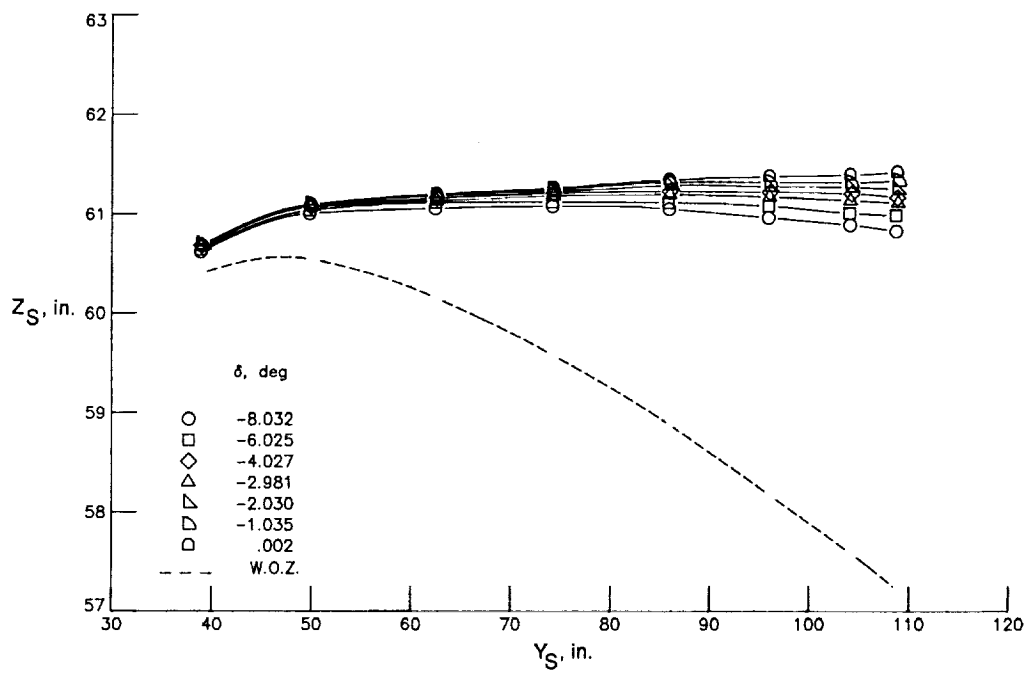
(a) Front spar; $\alpha = 0^\circ$.

Figure 11. Variation of wing front and rear spar shapes with control surface deflection at two angles of attack, $q = 100$ psf, and $M = 0.800$.



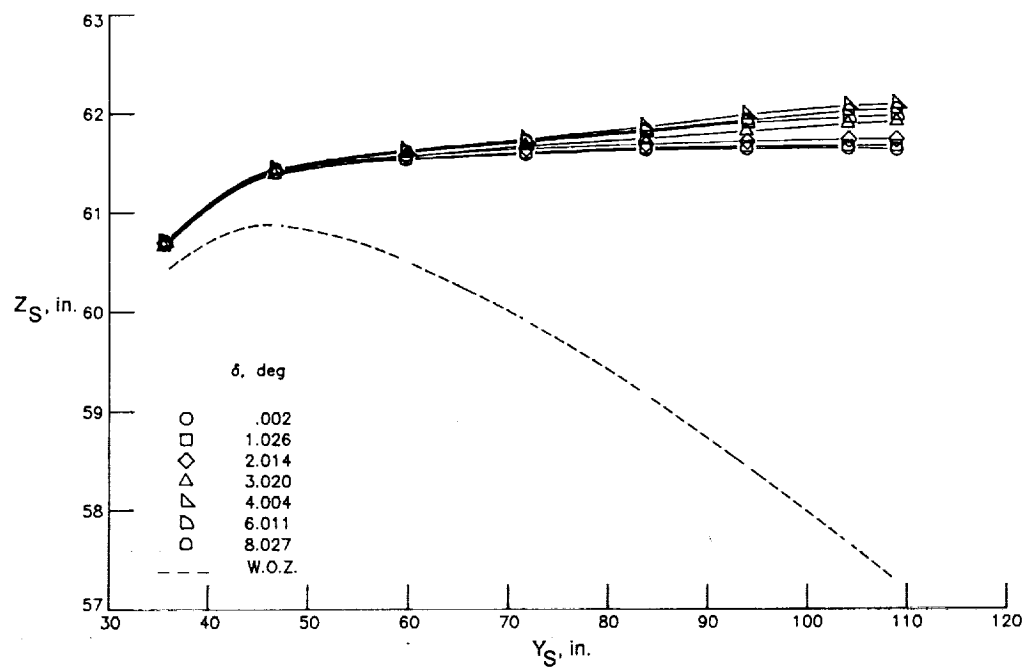
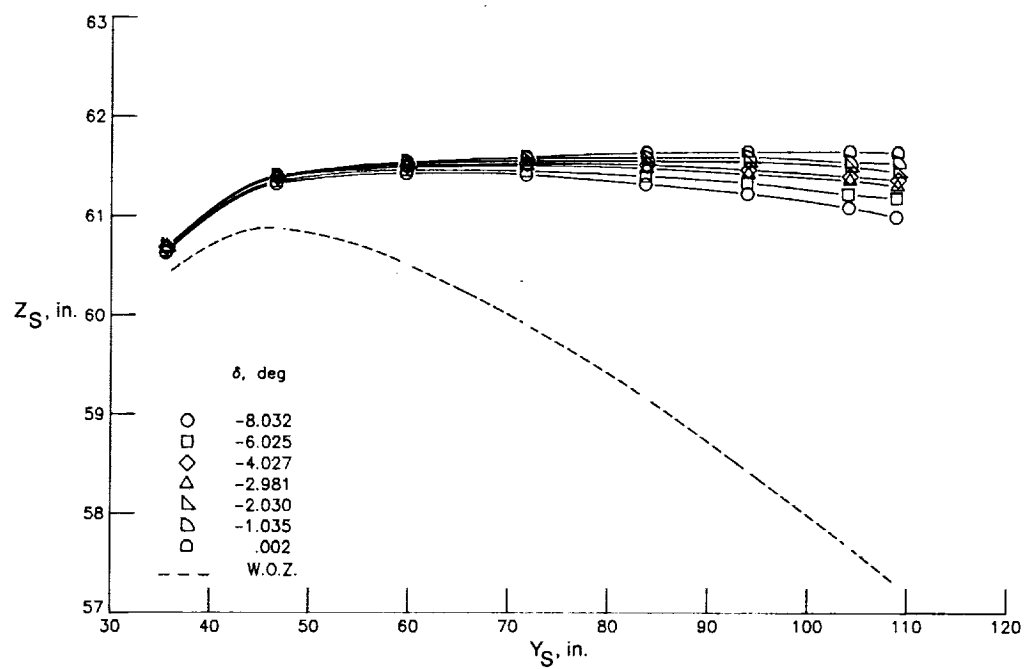
(b) Rear spar; $\alpha = 0^\circ$.

Figure 11. Continued.



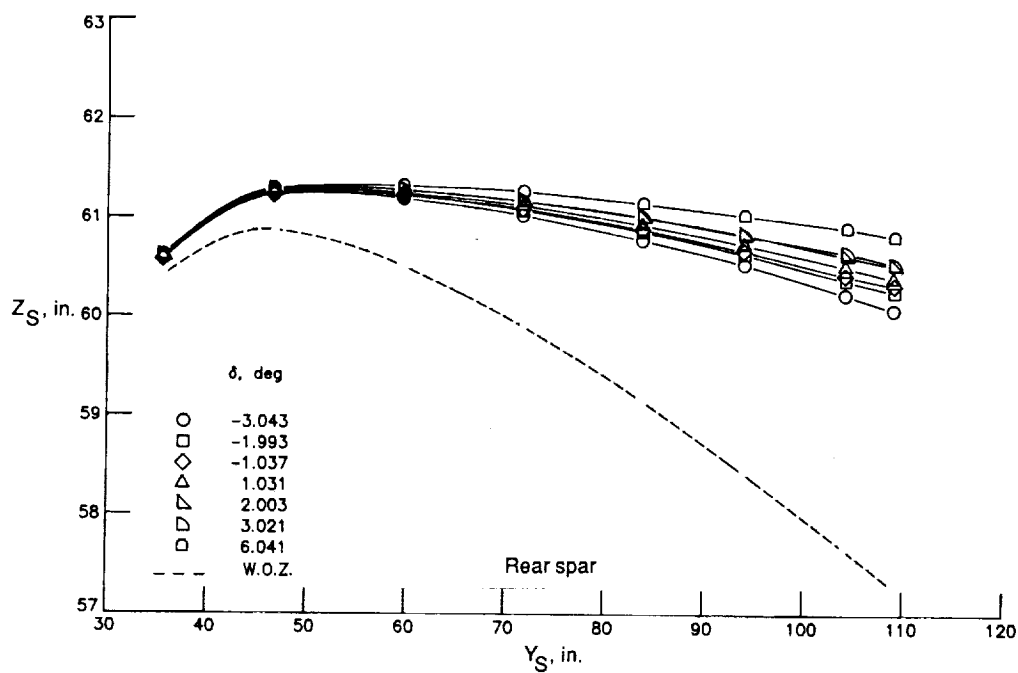
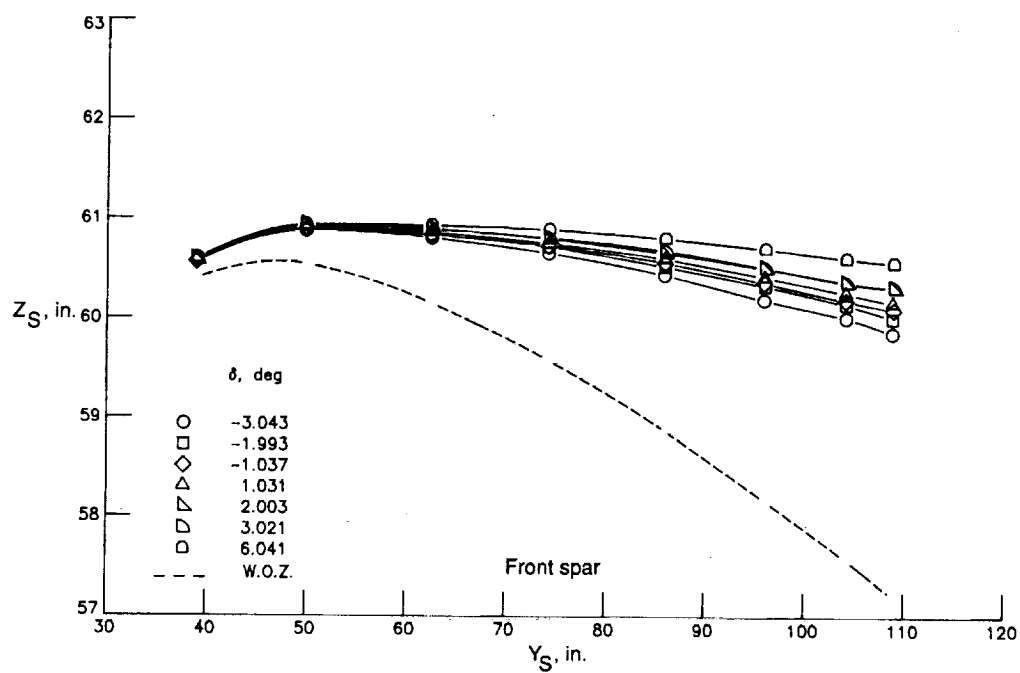
(c) Front spar; $\alpha = 2^\circ$.

Figure 11. Continued.



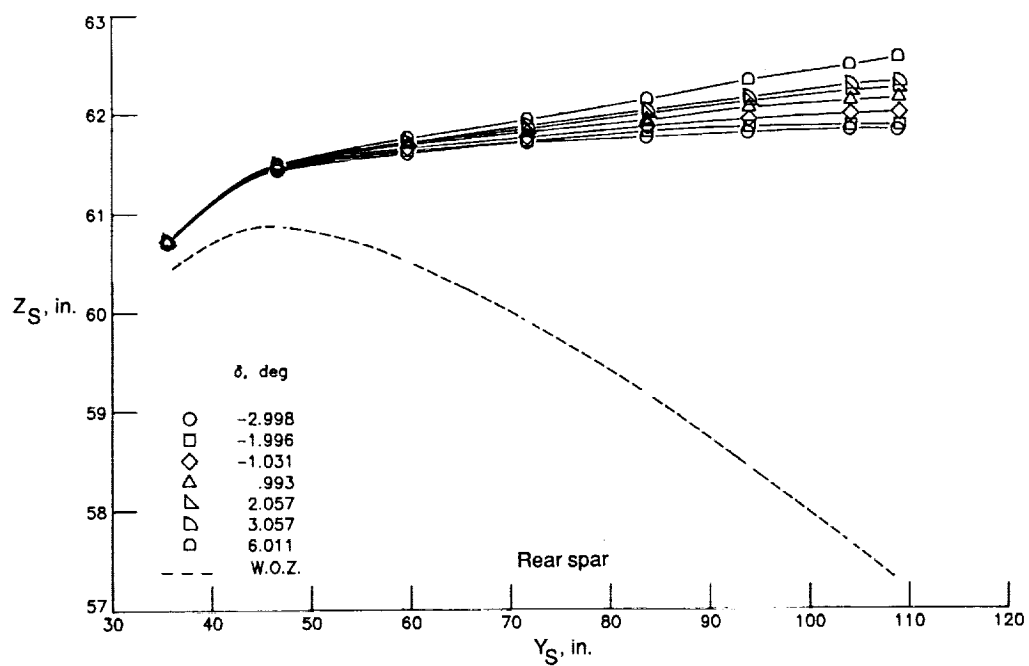
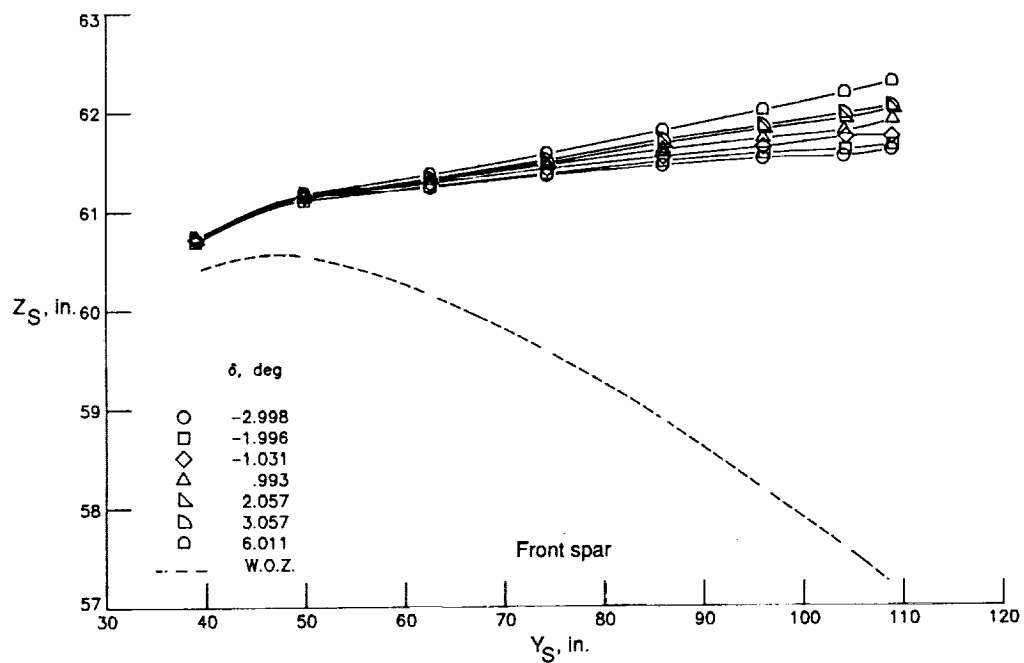
(d) Rear spar; $\alpha = 2^\circ$.

Figure 11. Concluded.



(a) $\alpha = 0^\circ$.

Figure 12. Variation of wing front and rear spar shapes with control surface deflection at two angles of attack, $q = 100$ psf, and $M = 0.850$.



(b) $\alpha = 2^\circ$.

Figure 12. Concluded.